BOREAS An international journal of Quaternary research

The geodynamic and limnological evolution of Balkan Lake Ohrid, possibly the oldest extant lake in Europe

BERND WAGNER, PAUL TAUBER, ALEXANDER FRANCKE, NIKLAS LEICHER, STEVEN A. BINNIE, ALEKSANDRA CVETKOSKA, ELENA JOVANOVSKA, JANNA JUST, JACK H. LACEY, ZLATKO LEVKOV, KATJA LINDHORST, KATERINA KOULI, SEBASTIAN KRASTEL, KONSTANTINOS PANAGIOTOPOULOS, ARNE ULFERS, DUŠICA ZAOVA, TIMME H. DONDERS, ANDON GRAZHDANI†, ANDREAS KOUTSODENDRIS, MELANIE J. LENG, LAURA SADORI, MIRKO SCHEINERT, HENDRIK VOGEL, THOMAS WONIK, GIOVANNI ZANCHETTA AND THOMAS WILKE

BOREAS

Wagner, B., Tauber, P., Francke, A., Leicher, N., Binnie, S. A., Cvetkoska, A., Jovanovska, E., Just, J., Lacey, J. H., Levkov, Z., Lindhorst, K., Kouli, K., Krastel, S., Panagiotopoulos, K., Ulfers, A., Zaova, D., Donders, T. H., Grazhdani, A.†, Koutsodendris, A., Leng, M. J., Sadori, L., Scheinert, M., Vogel, H., Wonik, T., Zanchetta, G. & Wilke, T. 2023 (January): The geodynamic and limnological evolution of Balkan Lake Ohrid, possibly the oldest extant lake in Europe. *Boreas*, Vol. 52, pp. 1–26. https://doi.org/10.1111/bor.12601. ISSN 0300-9483.

Studies of the upper 447 m of the DEEP site sediment succession from central Lake Ohrid, Balkan Peninsula, North Macedonia and Albania provided important insights into the regional climate history and evolutionary dynamics since permanent lacustrine conditions established at 1.36 million years ago (Ma). This paper focuses on the entire 584-m-long DEEP sediment succession and a comparison to a 197-m-long sediment succession from the Pestani site ~5 km to the east in the lake, where drilling ended close to the bedrock, to unravel the earliest history of Lake Ohrid and its basin development. $^{26}Al/^{10}Be$ dating of clasts from the base of the DEEP sediment succession implies that the sedimentation in the modern basin started at *c.* 2 Ma. Geophysical, sedimentological and micropalaeontological data allow for chronological information to be transposed from the DEEP to the Pestani succession. Fluvial conditions, slack water conditions, peat formation and/or complete desiccation prevailed at the DEEP and Pestani sites until 1.36 and 1.21 Ma, respectively, before a larger lake extended over both sites. Activation of karst aquifers to the east probably by tectonic activity and a potential existence of neighbouring Lake Prespa supported filling of Lake Ohrid. The lake deepened gradually, with a relatively constant vertical displacement rate of ~0.2 mm a^{-1} between the central and the eastern lateral basin and with greater water depth presumably during interglacial periods. Although the dynamic environment characterized by local processes and the fragmentary chronology of the basal sediment successions from both sites hamper palaeoclimatic significance prior to the existence of a larger lake, the new data provide an unprecedented and detailed picture of the geodynamic evolution of the basin and lake that is Europe's presumed oldest extant freshwater lake.

Bernd Wagner (wagnerb@uni-koeln.de), Paul Tauber, Niklas Leicher, Steven A. Binnie and Konstantinos Panagiotopoulos, Institute of Geology and Mineralogy, University of Cologne, Cologne 50674, Germany; Alexander Francke, Department of Earth Science, University of Adelaide, Adelaide 5005, South Australia, Australia; Aleksandra Cvetkoska, Department of Physical Geography, Utrecht University, Utrecht 3584 CB, The Netherlands and Department of Aquatic Ecology, Netherlands Institute of Ecology, Wageningen 6708 PB, The Netherlands; Elena Jovanovska, Department of Animal Ecology & Systematics, Justus Liebig University Giessen, Giessen 35392, Germany and Department of Palaeoanthropology, Senckenberg Research Institute, Frankfurt am Main 60325, Germany; Janna Just, Institute of Geology and Mineralogy, University of Cologne, Cologne 50674, Germany and Leibniz Centre for Tropical Marine Research, Bremen 28359, Germany; Jack H. Lacey, National Environmental Isotope Facility, British Geological Survey, Keyworth, Nottingham NG12 5GG, UK; Zlatko Levkov and Dušica Zaova, University Ss Cyril and Methodius, Institute of Biology, Skopje 1000, North Macedonia; Katja Lindhorst and Sebastian Krastel, Institute of Geosciences, Christian-Albrechts-University Kiel, Kiel 24118, Germany; Katerina Kouli, Faculty of Geology and Geoenvironment, National and Kapodistrian University of Athens, 15784 Zographou, Athens, Greece; Arne Ulfers and Thomas Wonik, Leibniz Institute for Applied Geophysics (LIAG), Hannover 30655, Germany; Timme H. Donders, Department of Physical Geography, Utrecht University, Utrecht 3508 TC, The Netherlands; Andon Grazhdani, Faculty of Geology and Mineralogy, University of Tirana, Tirana 1000, Albania; Andreas Koutsodendris, Institute of Earth Sciences, Heidelberg University, Heidelberg 69120, Germany; Melanie J. Leng, National Environmental Isotope Facility, British Geological Survey, Keyworth, Nottingham NG12 5GG, UK and Centre for Environmental Geochemistry, School of Biosciences, University of Nottingham, Loughborough LE12 5RD, UK; Laura Sadori, Dipartimento di Biologia Ambientale, Università di Roma "La Sapienza", Rome 00185, Italy; Mirko Scheinert, Institute of Planetary Geodesy, Technical University Dresden, Dresden 01069, Germany; Hendrik Vogel, Institute of Geological Sciences & Oeschger Centre for Climate Change Research, University of Bern, Bern 3012, Switzerland; Giovanni Zanchetta, Dipartimento di Scienze della Terra, University of Pisa, Pisa 56126, Italy; Thomas Wilke, Department of Animal Ecology & Systematics, Justus Liebig, University Giessen, Giessen, Germany; *received 26th April 2022, accepted 1st August 2022.* *†Deceased.*

Most of the oldest and deepest extant lakes on Earth are of tectonic origin and formed as graben lakes. Their long history has often promoted evolution of unique biota in the lake waters (Salzburger *et al.* 2014; Wilke *et al.* 2016) and allowed recording of climatic and environmental changes in their sedimentary successions back to Tertiary times (e.g. Kashiwaya *et al.* 2001; Brigham-Grette *et al.* 2013). Several of these lakes have been targeted by the International Continental Scientific Drilling Program (ICDP); e.g. Francke *et al.* (2017).

DOI 10.1111/bor.12601

Seismic site surveys have shown that the sedimentary fill in some of these lakes exceeds several hundred metres of thickness (e.g. Scholz *et al.* 1993; Niessen *et al.* 2007; Oberhänsli & Molnar 2012; Krastel *et al.* 2017 and references therein). However, only very few of the drilled sediment records from these lakes cover the entire lake history quasi-continuously and in high resolution, as technical or sedimentological limitations hampered drilling of the entire sedimentary successions. Moreover, chronological constraints of deeper sediments are often lacking and age estimations of these sediments are based on extrapolation of surface sedimentation rates (e.g. Krastel *et al.* 2017).

Lake Ohrid, at the border between North Macedonia and Albania (Fig. 1), is considered the oldest extant lake in Europe (with the possible exception of the Caspian Sea, which has a small European portion). It was the target of an ICDP drilling campaign in 2013 within the scope of the Scientific Collaboration on Past Speciation Condition in Lake Ohrid (SCOPSCO) project. The main goals of this project included unravelling the age and origin of the lake, reconstructing the regional climatic and environmental history and inferring the drivers of the high biodiversity and endemism in the area. So far, geological and (palaeo-)biological data are published from the upper 447 m core composite depth (m c.d.) of a 584-m-long sediment succession (5045–1 DEEP) recovered from the central part of the lake, where seismic data indicate the oldest and thickest sediment infill (Wagner *et al.* 2014). The upper 447 m c.d. comprise the entire hemi-pelagic, lacustrine sediment succession and thus the continuous existence of the lake since 1.364 million years ago (Ma) (Wagner *et al.* 2019). These studies focused on the paleoclimatic significance (Wagner *et al.* 2019) and on ecosystem dynamics and resilience (Panagiotopoulos *et al.* 2020; Wilke *et al.* 2020; Cvetkoska *et al.* 2021; Donders *et al.* 2021; Jovanovska *et al.* 2022). Based on hydro-acoustic data, the SCOPSCO project also provided new information on the geological history of the lake and particularly the tectonic activity (Fig. 1; Lindhorst *et al.* 2015). Biostratigraphical and seismic information from the DEEP site indicates that basin sediment infill started around 2.0 Ma, which is supported by genetic information from extant endemic species and molecular-clock analyses (Sušnik *et al.* 2006; Trajanovski *et al.* 2010; Lindhorst *et al.* 2015; Stelbrink *et al.* 2016, 2018; Wagner *et al.* 2017).

Despite a relatively good understanding of the environmental history of Lake Ohrid for the last 1.36 Ma, formation of the basin and the early stages of lake development remain poorly understood. This is partly due to the fact that previous studies focussed on the upper 447-m-long sediment succession from the DEEP site in the central part of the lake. The focus of this paper is on the geodynamic settings of the early basin and lake history, using the entire 584-m-long sediment succession from the DEEP site (5045–1) and a stratigraphical correlation to that from the nearby Pestani site (5045–4) in the central eastern part of the lake basin (Fig. 1). At the latter site, a 197-m-long sediment succession was recovered and drilling ended close to the bedrock. The comparison of granulometric, geochemical, geophysical, tephrostratigraphical, palaeomagnetic and biological data from both sites, in combination with seismic and borehole logging data, provides the foundation for unravelling the earliest lake history and basin development, the depth evolution of the lake, vegetation changes related to lake ontogeny, and the tectonic dynamics in the presumably oldest extant lake of Europe.

Material and methods

Site information and fieldwork

Lake Ohrid is located at 693 m above sea level (a.s.l.), has a maximum length of 30.4 km (N–S), a maximum width of 14.7 km (W–E), a surface area of 358 km^2, a tub-shaped bathymetry with a maximum water depth of 293 m, a mean water depth of ~151 m, and a total water volume of 50.7 km^3 (Fig. 1; Popovska & Bonacci 2007; Lindhorst *et al.* 2012). The catchment of Lake Ohrid is dominated by deciduous oak and hornbeam forests below 1250 m a.s.l., mixed mesophilous and montane forest between 1250 and 1800 m a.s.l., and sub-alpine grassland above (Donders *et al.* 2021 and references therein).

The selection of drill sites for the ICDP campaign at Lake Ohrid was based on two hydro-acoustic and seismic surveys in the years 2007 and 2008. Multi-channel seismic data were collected along ~500 km of profiles across the lake using a Mini GI Air Gun (0.25 L in 2007 and 0.1 L in 2008) and a 16-channel 100-m-long streamer. More details on the technical settings and the locations of the profiles are given in Lindhorst *et al.* (2015). Processing of seismic data followed standard procedures and included the setup of the geometry, editing of bad traces, band pass filtering (frequency: 35/60–600/900 Hz), normal moveout (NMO) correction, stacking, and a finite-difference time migration. A predictive deconvolution aimed at the suppression of multiples; however, multiples are clearly visible in the processed data. A constant velocity of 1600 m s^{-1} was used for the conversion of two-way travel time to sediment thickness in m.

At the drill site DEEP (latitude 41°02′57″N, longitude 020°42′54″E) at 243 m water depth in the central part of the lake (Fig. 1) seismic data showed a maximum sediment fill of ~680 m below lake floor (b.l.f.) for the lake basin (Fig. 2; Wagner *et al.* 2014). At this site, four parallel holes were drilled to a maximum depth of 568.9 m b.l.f., where the occurrence of very coarse gravel and cobbles hindered further penetration (Wagner *et al.* 2014). The correlation of core segments from the

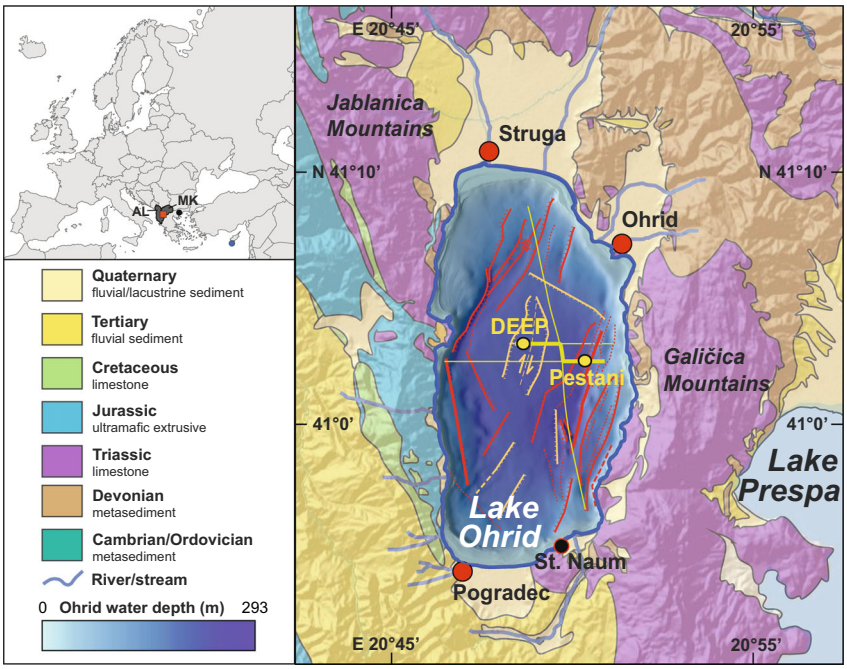

Fig. 1. Map of Lake Ohrid and its surrounding area, with geology, topography and bathymetry of the lake (compiled from Wagner *et al.* 2019 and Wilke *et al.* 2020), cities (red dots), St. Naum (black dot) and the locations of the DEEP and Pestani drill sites (yellow dots). The locations of selected seismic profiles (yellow), major active faults (red) and inactive faults (orange) are from Lindhorst *et al.* (2015); thick yellow sections indicate seismic profiles shown in Fig. 2. The overview map (left) marks the locations of Lake Ohrid (red square) at the boundary between North Macedonia (MK, dark grey right) and Albania (AL, dark grey left), the Tenaghi Philippon pollen record (black dot) and ODP Site 967 (blue dot).

individual holes was established using optical information, lithological and geochemical data (Francke *et al.* 2016). The composition of individual segments and sediment expansion due to gas expansion led to a total core composite length of 584 m, with a recovery of 99% for the upper 430 m and 95% for the entire succession. The Pestani drill site (41°02′20.80″N, 020°45′44.50″E), at a water depth of 262 m in the central eastern part of the lake floor (Fig. 1), was selected with the aim of reaching sediments deposited directly above the bedrock at ~200 m b.l.f. (Fig. 2). At this site, only one hole was drilled down to 195 m b.l.f. with a core recovery of 91% (Wagner *et al.* 2014). As sediment expansion was moderate and all cores came from the same hole, the length of the composite sediment succession is 197 m c.d. and exceeds only slightly the maximum drill depth.

After finishing drilling at the DEEP and Pestani sites, geophysical downhole logging was carried out, and continuous data sets of sedimentary physical properties were acquired at both sites (Baumgarten *et al.* 2015; Ulfers *et al.* 2022). Logging details, probes and data processing are described in detail in Baumgarten *et al.* (2015) and Ulfers *et al.* (2022). Among various probes, a spectral gamma ray (SGR) probe was run through the drill pipe at a logging speed of 3 m min^{-1} and a sampling interval of 10 cm, which allows a vertical resolution of approximately 10–20 cm, and records the total gamma radiation (GR), as well as the spectral components (potassium, thorium and uranium) and their contribution to the GR (Baumgarten *et al.* 2015).

Laboratory work

Analyses of sediment from Lake Ohrid comprise a broad suite of granulometric, geochemical, geophysical, tephrostratigraphical, palaeomagnetic and biological methods (e.g. Cvetkoska *et al.* 2016; Francke *et al.* 2016; Jovanovska *et al.* 2016; Just *et al.* 2016, 2019; Lacey *et al.* 2016; Leicher *et al.* 2016, 2019; Sadori *et al.* 2016; Zanchetta *et al.* 2018; Koutsodendris *et al.* 2019; López-Blanco *et al.* 2020; Thomas *et al.* 2020; Zaova *et al.* 2022). Published data from the DEEP sediment succession so far are restricted to the upper 447 m c.d., where fine-grained sediments document the entire history of permanent lacustrine conditions for Lake Ohrid (Wagner *et al.* 2019). Based on tephrochronological tie points, tuning of the total organic carbon content in the sediments vs. orbital parameters, and validation by palaeomagnetic events, a Bayesian age-depth model was established. This model shows that the upper 447 m c.d. of the DEEP sediment succession comprise the last 1.364 Ma (Wagner *et al.* 2019). Some of these analytical methods are herein extended to the base of the 584-m-long sediment succession from the DEEP site and are now also applied to the 197-m-long sediment succession from the Pestani site.

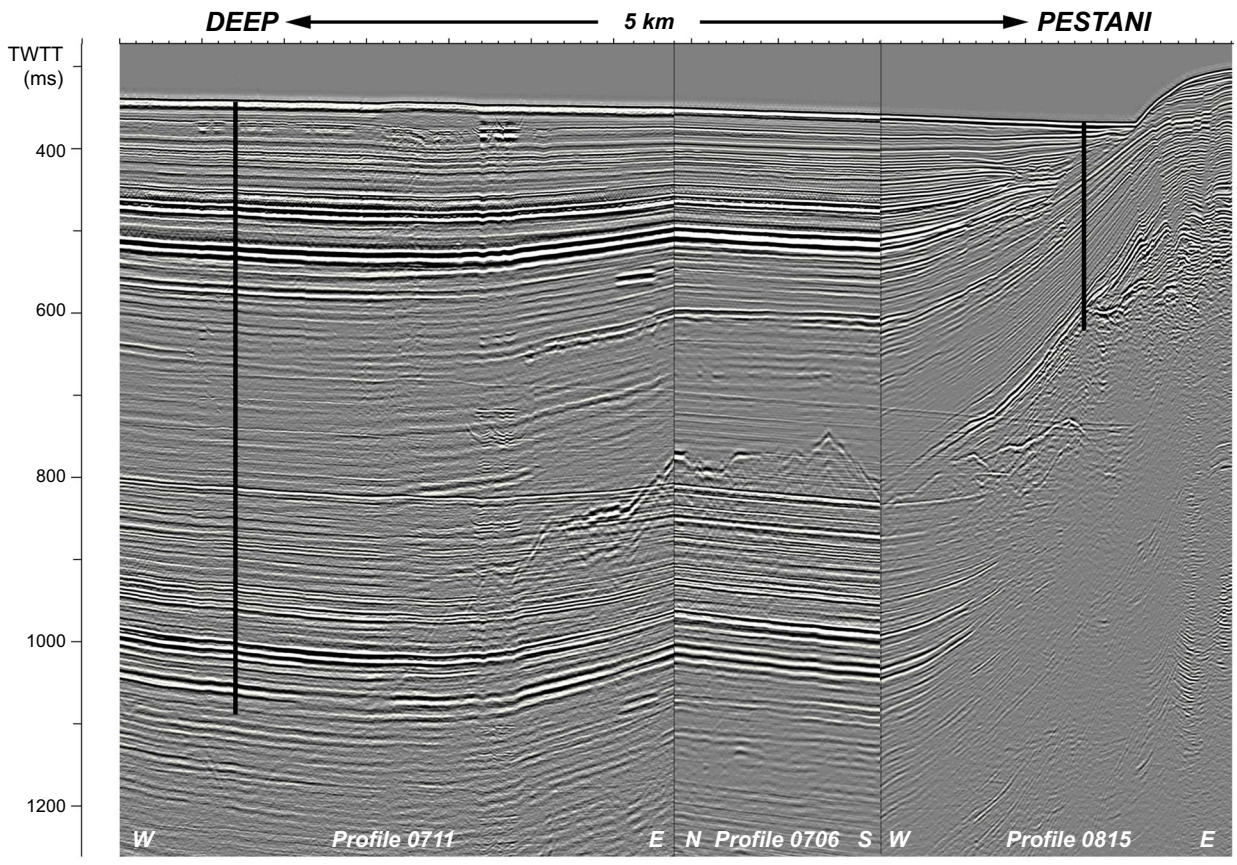

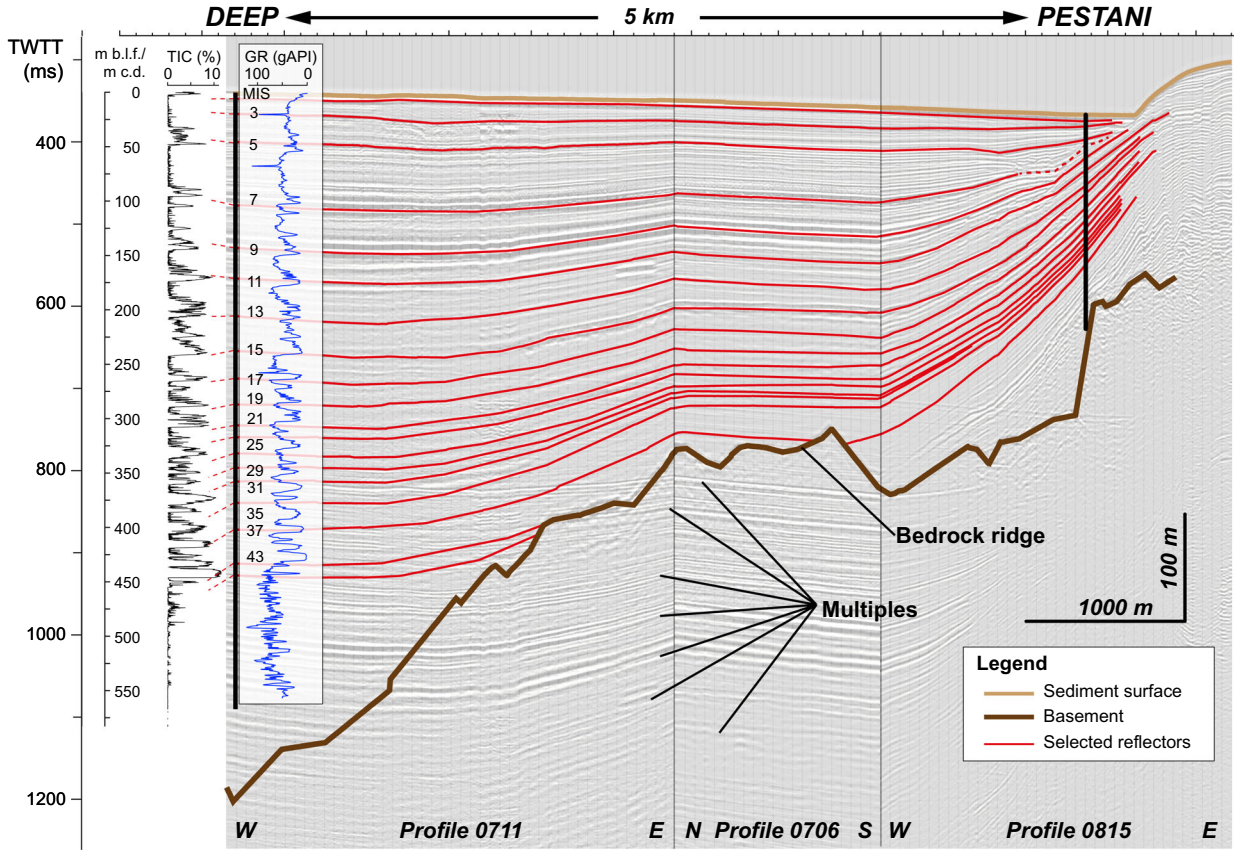

Fig. 2. Composite seismic profile from the DEEP site to the Pestani site; for location see Fig. 1. The location of the drill sites and the depth of the drilling are indicated by the black vertical lines. Total inorganic carbon (TIC) from sedimentological analyses and natural gamma radiation (GR, inverse scale) from borehole logging with correlating marine isotope stages (MIS) are displayed close to the DEEP site record. Note that GR is plotted vs. metres below lake floor (m b.l.f.), whereas TIC data are plotted vs. metres composite depth (m c.d.), which differ due to core expansion and composition of cores from different boreholes at the DEEP site. Red lines indicate prominent reflectors and their position relative to the borehole logging data, MIS and TIC data. Note that primary reflectors interfere with multiples at greater subsurface depths. Depth conversion from two-way travel time (TWTT) from the seismic data into m b.l.f. and m c.d. follows Ulfers *et al.* (2022).

The published and new data sets are indicated in the individual method descriptions.

Granulometric analyses followed the methods described in Francke *et al.* (2016) and were applied to and have been published for the DEEP sediment succession down to 447 m c.d. (e.g. Wagner *et al.* 2019; Wilke *et al.* 2020). For this paper, the data set from the DEEP site was extended to 584 m c.d., with a sample resolution of 64 cm, if there were no gaps. The same methods were also applied to the Pestani sediment succession. Sample resolution averages 50 cm, with a reduced resolution being necessary for the lower part of the record where more gaps are present (Wagner *et al.* 2014). After removal of lacustrine sediment components, such as authigenic calcite, organic and silicaceous matter, samples were dispersed using $Na_4P_2O_7$, placed in a shaker for 12 h, and then subjected to 1 min of ultrasonic treatment. Sample aliquots were then measured three times with a Beckmann Coulter 13320 laser particle analyser. The individual results were averaged and then processed using the GRADISTATv8 program (Blott & Pye 2001).

Geochemical analyses included elemental analyses and XRF scanning, followed the methods described in Francke *et al.* (2016) were applied to and have been published for the DEEP sediment succession down to 447 m c.d. (e.g. Wagner *et al.* 2019; Wilke *et al.* 2020). XRF scanning was carried out with an ITRAX® core scanner, which was equipped with a chromium (Cr) X-ray source and was run at 30 kV and 30 mA. Scanning steps were set to 2.5-mm resolution with an integration time of 10 s and were also applied to the DEEP sediment succession below 447 m c.d. and to the entire Pestani sediment succession. Total carbon (TC) and total inorganic carbon (TIC) were determined as released CO_2 after sample aliquots were dispersed in 10 mL DI water and using a DIMATOC 100 carbon analyser (Dimatec®). Sample resolution was 8 and 16 cm for the upper 447 m c.d. of the DEEP sediment succession (e.g. Wagner *et al.* 2019), which was now also applied to the succession below 447 m c.d. For the Pestani sediment succession sample resolution was set to 24 cm if there were no gaps in recovery. TC was measured after combustion at 900 °C and TIC was determined after sample aliquots were treated with phosphoric acid (H_3PO_4) and combusted at 160 °C. Total organic carbon (TOC) was calculated as the difference between TC and TIC. Total nitrogen (TN) was analysed using a vario MICRO cube (Elementar®). Oxygen and carbon isotope ratios ($\delta^{18}O$ and $\delta^{13}C$) were measured on carbonate according to the protocol described in Lacey *et al.* (2016) and have been published for the DEEP sediment succession down to 447 m c.d. (e.g. Wagner *et al.* 2019; Panagiotopoulos *et al.* 2020; Wilke *et al.* 2020). Bulk carbonate samples were taken at intervals of 16 cm from the DEEP sediment succession for the upper 447 m c.d. This interval was now also taken for the DEEP sediment succession below 447 m c.d., where carbonate content was >0.5% and comprises calcite (Lacey *et al.* 2016). For the period of interest of this paper, bulk carbonate samples from the Pestani sediment succession between 133 and 180 m c.d. were taken accordingly at intervals of 24 cm. Sample pretreatment included removal of organic material using sodium hypochlorite, sieving at 64 µm to remove shell material, and the reaction of fine fraction carbonate for 16 h with anhydrous phosphoric acid at 25 °C. The CO_2 yield was separated cryogenically from water vapour and then analysed using a VG Optima dual inlet mass spectrometer. The oxygen and carbon isotope compositions of calcite ($\delta^{18}O_C$ and $\delta^{13}C_C$, respectively) are reported in delta notation (δ) as per mille (‰) deviations of the isotope ratios $^{18}O/^{16}O$ and $^{13}C/^{12}C$ calculated to the VPDB scale. Within-run laboratory standards with known values calibrated to international reference materials NBS19 and NBS18 were utilized for which analytical reproducibility was <0.1‰ for $\delta^{18}O$ and $\delta^{13}C$.

Tephrostratigraphical methods and results from the DEEP site sediment succession down to 447 m c.d. are described in Leicher *et al.* (2019, 2021). In the upper 412.4 m c.d., 57 tephra layers were found and investigated for their morphological appearance, geochemical fingerprint, and (chrono-)stratigraphical position. No tephra was found below 412.4 m c.d. (Leicher *et al.* 2021). Tephrostratigraphical methods applied to the new Pestani sediment succession followed these methods. Within the upper 140 m c.d. of the Pestani sediment succession, 31 tephra layers were identified during visual core description and subsequent high-resolution line-scan image inspection (Table S1). Tephra layers were labelled according to the prefix scheme: OH (Ohrid) – PE (Pestani) or DP (DEEP) – and followed by sample depth in dm. Individual glass fragments of tephra layers were separated and analysed for their major and minor element compositions using electron microprobe analysis wavelength dispersive spectroscopy (EMPA-WDS) (Leicher 2021; Leicher *et al.* 2021). The full data set of tephra layers and secondary reference materials analysed is available at the EarthChem repository

(https://ecl.earthchem.org/view.php?id=2292). Tephra layers of the DEEP and Pestani sites were correlated based on their geochemical fingerprints and respective lithostratigraphical and stratigraphical information (Figs S1–S12, Data S1).

Magnetic measurements for the upper 447 m c.d. of the DEEP sediment succession are described in Just *et al.* (2016, 2019). From the DEEP sediment succession, measurements were performed after the first screening of low-resolution samples (mainly 48-cm increments) on continuously subsampled intervals across detected polarity transitions of the Matuyama–Brunhes boundary and the base of the Jaramillo subchron (Just *et al.* 2019). The low-resolution data set was now extended to the base of the DEEP sediment succession. From the new Pestani sediment succession, 89 samples (i.e. mainly 48-cm increments) were analysed from the interval 89–135 m c.d. Measurements of the natural remanent magnetization (NRM) and stepwise alternating field (AF) demagnetization up to 100 mT were carried out using 2G Enterprises cryogenic magnetometers at 10 incremental steps. Following the former studies on the DEEP sediment succession the imprint of greigite on palaeomagnetic data was quantified by the ratio between the so-called gyro-remanent magnetization (GRM) and NRM, i.e. ΔGRM/ΔNRM. The maximum angular deviation (MAD) was calculated to provide a measure of the quality of demagnetization data (see Just *et al.* 2016, 2019 for details). Data of samples acquiring a significant GRM (>10% of NRM) and with MADs >10° were discarded.

Pollen analyses for the sediment succession from 400–447 m c.d. in the DEEP site (1.16–1.36 Ma) were performed on 103 samples in intervals down to 16 cm intervals (Panagiotopoulos *et al.* 2020). An average pollen sum of 998 terrestrial pollen grains (515 excluding *Pinus*), spores, obligate aquatics, and algae were counted per sample to ensure recording of rare pollen taxa in specific relict species (for details see Sadori *et al.* 2016; Kousis *et al.* 2018; Panagiotopoulos *et al.* 2020; Donders *et al.* 2021). For this paper, 20 additional samples from 447–510.48 m c.d. of the DEEP site were processed and analysed. Only 10 of these samples yielded palynomorph concentrations worth investigating and 7 of these (down to 468.4 mc.d.) have an average pollen sum of 285 terrestrial pollen grains (203 excluding *Pinus*). This extended DEEP data set was compared to the interval of 133.35–179.95 m c.d. from the Pestani sediment succession, where borehole logging data (Ulfers *et al.* 2022) and core catcher material (Wagner *et al.* 2014) infer the transition to permanent lacustrine conditions. A total of 30 samples from the Pestani site were processed and analysed following the methods from the DEEP site. A total of 27 samples contained sufficient palynomorph concentrations and yielded an average pollen sum of 800 terrestrial pollen grains (473 excluding *Pinus*). This allowed us recording of rare pollen taxa in specific relict species.

Processing of sediment samples for diatom analyses and preparation of permanent diatom slides followed the methods by Cvetkoska *et al.* (2014). For the upper 447 m c.d. of the DEEP site record, 380 sediment samples were taken at a temporal resolution of 2–4 ka and data are published (e.g. Panagiotopoulos *et al.* 2020; Wilke *et al.* 2020; Jovanovska *et al.* 2022). For this paper, another 125 sediment samples were selected at intervals between 0.64 and 1.6 m in the sediment succession from below 447 m c.d. In this part of the DEEP site record, total diatom counts decreased substantially and only 32 samples contained diatoms, some with only a single diatom. Below 510 m c.d. of the DEEP site record, only five samples contained up to five diatom valves. Because contamination or sediment reworking cannot be excluded, these samples were not included in the analyses. From the new Pestani record, 22 sediment samples were selected for diatom counting at intervals between 0.48 and 8.74 m in the sediment succession between 126 and 174 m c.d. No diatoms were found below 174 m c.d. Permanent diatom slides were prepared using Naphrax® as a mountant and each slide was analysed across random transects to count 200–400 diatom valves, wherever possible (see Wilke *et al.* 2020 for details). Diatom analyses were conducted at 1000 and 1500× magnification. Following the approach of Panagiotopoulos *et al.* (2020), diatom taxa were categorized into five depth classes according to their habitat preferences and spatial distribution in the lake: 0–5 m (shallow littoral communities), 0–10 m (littoral communities), 0–40 m (epilimnetic planktonic and sublittoral communities), and 20–80 m (hypolimnetic planktonic communities).

Burial dating using in situ-produced cosmogenic $^{26}Al/^{10}Be$ (e.g. Granger & Muzikar 2001) was performed on 10 individual samples comprised of eight quartz-rich pebbles, plus two samples of amalgamated sediments sieved to either the granule or coarse/very coarse sand size fractions. These samples were extracted for this paper from 586.18–585.64 m c.d. of the DEEP sediment succession. Following crushing and sieving of the samples to 250–500 μm, pure quartz separates ranging from 2 to 40 g were obtained using the etching procedure of Kohl & Nishiizumi (1992), which in the case of the small pebbles was modified to prevent quartz loss by performing the first two dilute HF/HNO_3 etches on the whole sample before crushing and then etching the crushed sample once more. Purity checks on assays of the cleaned quartz were undertaken in-house using inductively coupled plasma optical emission spectrometry (ICP-OES). Samples were spiked prior to dissolution with commercially available Be and Al ICP standard solutions (Scharlab, 1000 mg L^{-1}). Subsequent preparation as accelerator mass spectrometry (AMS) targets at the University of Cologne followed the stacked column

approach outlined in Binnie *et al.* (2015). The samples were prepared in two batches, each additionally containing one chemical blank. Targets were measured on CologneAMS (Dewald *et al.* 2013), with $^{10}Be/^{9}Be$ and $^{26}Al/^{27}Al$ ratios normalized to the standards of Nishiizumi *et al.* (2007) and Nishiizumi (2004), respectively.

State of the art

According to former geological studies and seismic data obtained during the site surveys of the SCOPSCO project, the Ohrid basin formation initiated as a pull apart basin during a transtensional phase in the Late Miocene followed by an extensional phase since the Pliocene (Dumurdzanov *et al.* 2004, 2005; Burchfiel *et al.* 2006; Lindhorst *et al.* 2015; Pashko & Aliaj 2020). The deposition of the lowermost sedimentary units recognized in the seismic data was ascribed to the first phase of the syn-rift stage of basin evolution, when a transient narrow valley may have been filled quickly by a fluvial system and small sub-basins formed by progressive extension (Lindhorst *et al.* 2015 and references therein). According to biostratigraphical and seismic information and extrapolation of sedimentation rates from the DEEP site, this basin sediment infill may have started around 2.0 Ma (Lindhorst *et al.* 2015; Wagner *et al.* 2017). The lake has existed continuously since 1.364 Ma, which is evidenced by combining information from seismic (Lindhorst *et al.* 2015), borehole logging (Ulfers *et al.* 2022) and sedimentological data (Wagner *et al.* 2019). Mass wasting in the lateral parts of the lake is common and can be related to tectonic activity and earthquakes (Wagner *et al.* 2008, 2012b; Reicherter *et al.* 2011; Lindhorst *et al.* 2012). Active and inactive faults within Lake Ohrid are mainly oriented in NE–SW directions (Fig. 1).

Sedimentological data comprising the early lake history are so far published only from the upper 447 m c.d. of the DEEP site sediment succession and are thus restricted to the entire hemi-pelagic, lacustrine sediment succession deposited since the continuous existence of the lake. These data allowed for a better understanding of the influence of the African monsoon on winter rainfall in the northern Mediterranean region (Wagner *et al.* 2019) and on the regional vegetation succession and the evolution of the young Lake Ohrid ecosystems and their ecosystem resilience (Panagiotopoulos *et al.* 2020; Donders *et al.* 2021). Moreover, the continuous species-level fossil record of diatoms from Lake Ohrid along with environmental and climate indicator time series gave new insights into the evolutionary and community dynamics of an isolated ecosystem since its formation (Wilke *et al.* 2020; Cvetkoska *et al.* 2021; Jovanovska *et al.* 2022).

Based on the former studies of the DEEP site sediment succession, TIC in Lake Ohrid sediments is known to result mainly from endogenic calcite precipitation in lake surface waters. Abundance variations of TIC reflect temperature and precipitation changes at Lake Ohrid primarily on orbital time scales (Wagner *et al.* 2019), with high values during interglacial periods (Fig. 3). K intensities represent the amount of terrigenous clastic matter in the sediments and thus are negatively correlated to TIC and the amount of organic matter (e.g. Francke *et al.* 2016; Wagner *et al.* 2019; Wilke *et al.* 2020). TOC and TN data represent the amount of organic material in the sediments and were used, in combination with tephrostratigraphical and palaeomagnetic data, for the establishment of the age-depth model at the DEEP site back to 1.36 Ma (Francke *et al.* 2016; Just *et al.* 2019; Wagner *et al.* 2019; Leicher *et al.* 2021). The TOC/TN ratio can be used to differentiate between autochthonous and allochthonous organic matter supply (e.g. Meyers & Ishiwatari 1995), but it can also be affected by other factors, such as selective loss of C or N during and after sedimentation (e.g. Lehmann *et al.* 2002; Francke *et al.* 2016). Grain-size data provide information on lake internal transport energy. As Lake Ohrid is mainly fed by karst aquifers (e.g. Matzinger *et al.* 2007; Lacey & Jones 2018) and major inlets do not occur along the central eastern shore (Fig. 1), variations in grain-size data may reflect lake-level changes, lake internal current activity, or aeolian input (cf. Vogel *et al.* 2010b). Diatom data provided information on habitat heterogeneity, trophic state and changing water depths (e.g. Wilke *et al.* 2020; Cvetkoska *et al.* 2021; Jovanovska *et al.* 2022). Pollen provided regional information on vegetation and ecology changes in the catchment (e.g. Sadori *et al.* 2016; Panagiotopoulos *et al.* 2020; Donders *et al.* 2021) and stable isotopes provided information on lake water sourcing and changes in the evaporation vs. precipitation ratio (e.g. Lacey *et al.* 2015, 2016). The combination of information from the published data set of the DEEP site sediment succession shows that expansion and deepening of Lake Ohrid was gradual, and deeper water conditions had established at this site around 1.15 Ma (Wilke *et al.* 2020).

Stratigraphical correlation of DEEP and Pestani records

The stratigraphical correlation of the DEEP and Pestani sites is mainly based on seismic and sedimentological data (Figs 2, 3). Independent stratigraphical tie points between the DEEP and Pestani sites are provided by the occurrence of tephra layers identified in the sediment successions from both sites (Tables 1, S1) and by palaeomagnetic reversals and excursions. Borehole logging data support the stratigraphical correlation, particularly in the lower sediment successions where some gaps occur.

A stratigraphical correlation based on seismic data follows three profiles across Lake Ohrid, two of them

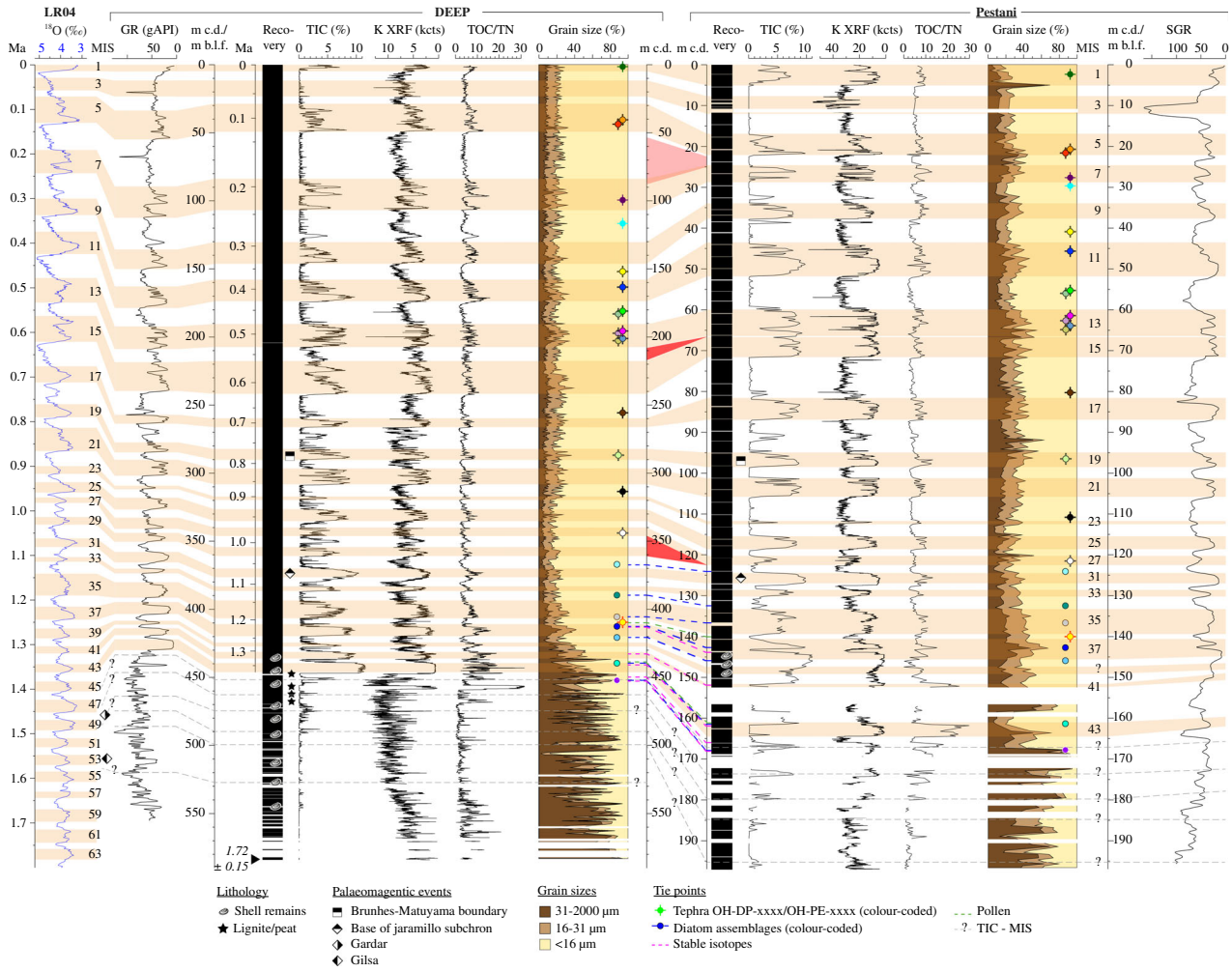

Fig. 3. Correlation of benthic isotope stack LR04 and MIS boundaries (Lisiecki & Raymo 2005), natural gamma radiation (GR, inverse scale) from borehole logging (Ulfers *et al.* 2022) and TIC, K from XRF scanning, TOC/TN ratio, and grain sizes in the DEEP and Pestani sediment successions. Ages and data from the DEEP site back to 1.36 Ma are from Francke *et al.* (2016), Wagner *et al.* (2019) and Wilke *et al.* (2020), with the TOC/TN ratio so far only published back to 640 ka (Francke *et al.* 2016). Locations of tephra horizons in the DEEP sediment succession are from Leicher *et al.* (2021) and correlation to respective layers (colour-coded) in the Pestani sediment succession is shown in more detail in Fig. 4, Tables 1 and S1. Ages from palaeomagnetic excursions Gardar and Gilsa (left) are from Chanell (2017). The age at the base of the DEEP site succession (black triangle) is from $^{26}Al/^{10}Be$ burial dating (Table S2). Diatom (see also Fig. 6), pollen (see also Fig. 7) and stable isotope data (see also Fig. 8) complement the stratigraphical correlation in the lower part of the DEEP and Pestani sediment successions. Major hiatuses in the sediment successions are indicated by gaps in the recovery logs and red triangles between the two sites.

roughly in W–E direction and one interjacent in N–S direction (thick yellow lines in Fig. 1). According to the seismic data, the sediment layers at the DEEP site are well stratified and show fairly horizontal bedding, whilst the geological situation in the eastern part of the basin is more complex (cf. Lindhorst *et al.* 2015). Disrupted and tilted reflectors occur directly west of the Pestani site (Fig. 2). They indicate tectonic activity, mass wasting and/or distinctly changing sedimentation rates and impede tracing of some reflectors between the DEEP and Pestani sites, particularly at intermediate depths (Fig. 2). Tracing of the deepest reflectors is also hindered in the central basin, including areas around the DEEP site, where multiple reflectors interfere with primary reflections. Moreover, a bedrock ridge in the eastern part of the basin interrupts the deepest sedimentary reflectors. Despite these difficulties, selected horizons can be well traced from the DEEP to the Pestani site, as has already been shown for some horizons with ages of <1 Ma (Ulfers *et al.* 2022), and thus support the correlation based on sedimentological data.

For a stratigraphical correlation between the DEEP and Pestani sites based on sedimentological data, we used different proxy data sets, as deeper waters likely diminish local effects on sedimentary characteristics. The published data from the DEEP site show that deeper water conditions had established at this site around 1.15 Ma (Wilke *et al.* 2020). Therefore, we split the

Table 1. Tephra layers found in the DEEP sediment succession and their equivalents in the Pestani sediment succession. Tephra ages of the DEEP site are based on the chronology presented in Wagner *et al.* (2019). Correlated equivalents according to Leicher *et al.* (2016, 2019, 2021). ET = Etna; CF = Campi Flegrei; CVZ = Campanian Volcanic Zone; RMF = Roccamonfina; SVD = Sabatini Volcanic District; CA = Colli Albani.

DEEP				Pestani			Correlative equivalents
Label	Isochrone depth (m c.d.)	Thickness (cm)	Age (ka)	Label	Isochrone depth (m c.d.)	Thickness (cm)	
OH-DP-0015	1.554	Crypto	3.29±0.08	OH-PE-0024	2.48	Crypto	ET; FL tephra
OH-DP-0404	40.486	3.00	102.11±3.09	OH-PE-0208	20.87	3.00	CF; Tm24a/POP2
OH-DP-0435	43.513	1.50	109.45±1.82	OH-PE-0214	21.46	0.80	CF; X-6
OH-DP-0977	99.723	2.00	228.87±5.66	OH-PE-0273.9	27.39	0.50	CVZ/RMF?; S3?
OH-DP-1175	117.543	2.50	270.64±4.88	OH-PE-0294.8	29.48	0.50	SVD; unknown
OH-DP-1527	152.773	1.50	358.25±4.64	OH-PE-0402	40.20	1.80	RMF; unknown
OH-DP-1640	164.086	2.00	398.37±5.95	OH-PE-0452	45.26	3.40	RMF; unknown
OH-DP-1812	181.241	1.20	453.95±2.94	OH-PE-0565	56.56	0.90	RMF; unknown
OH-DP-1817	181.769	2.50	456.19±3.30	OH-PE-0569	56.98	2.70	CA; Pozzolane Rosse
OH-DP-1955	195.566	3.00	490.67±3.92	OH-PE-0616	61.64	3.20	RMF; unknown
OH-DP-1966	196.646	3.00	494.05±4.43	OH-PE-0622	62.20	2.40	RMF; CES1/A2
OH-DP-2010	201.049	1.50	514.17±4.37	OH-PE-0642	64.24	3.80	RMF; SC5/A7
OH-DP-2017	201.782	3.50	516.87±5.47	OH-PE-0648	64.88	3.10	SVD; Fall A
OH-DP-2555	255.586	2.40	662.55±7.16	OH-PE-0801	80.19	3.20	CVZ?; A11/12
OH-DP-2869	286.915	2.00	776.51±5.14	OH-PE-0965	96.56	1.40	CVZ?; unknown
OH-DP-3144	314.402	4.30	888.18±5.28	OH-PE-1111	111.10	0.80	CVZ?; unknown
OH-DP-3443	344.394	0.80	979.33±6.19	OH-PE-1213	121.39	1.60	CVZ?; unknown
OH-DP-4089	408.989	1.80	1206.9±4.55	OH-PE-1400	140.03	0.80	CVZ?; unknown

stratigraphical correlation between the DEEP and Pestani sites into the period <1.15 Ma, corresponding with the transition from Marine Isotope Stage (MIS) 34 to MIS 35 (Lisiecki & Raymo 2005), and the prior period, when environmentally dynamic and relatively shallow water conditions, fluvial conditions or peat formation prevailed at the DEEP site (Wagner *et al.* 2014; Panagiotopoulos *et al.* 2020; Wilke *et al.* 2020). A correlation of sediment proxies >1.15 Ma can provide information on the existence of a larger water body that connected the DEEP and Pestani sites, periods of isolated water bodies or even desiccation at both sites, deepening of the early Lake Ohrid, distance of coring sites to shore, and onset of sedimentation in the Ohrid basin.

Stratigraphical correlation back to 1.15 Ma

For the stratigraphical correlation based on sedimentological data back to 1.15 Ma, we selected TIC, K counts from XRF scanning, the TOC/TN ratio and grain-size information. Variations of the TOC/TN between the DEEP and Pestani sites can be assumed to be negligible, as lake internal currents (cf. Wagner *et al.* 2008; Vogel *et al.* 2010a) mix the organic material in the water column sufficiently at the centennial time scale. Variations in grain-size data are assumed to be relatively similar at both sites, once pelagic water conditions were established. This is also assumed for diatom data, which complement the stratigraphical correlation between the DEEP and Pestani sites in the lowermost sections of the period <1.15 Ma.

For the period <1.15 Ma, the MIS31 interglacial at 1.081–1.062 Ma (Lisiecki & Raymo 2005), characterized by its exceptionally warm conditions, is a key tie point represented in the DEEP sediment succession by a prominent maximum in TIC at 375 m c.d. (Wagner *et al.* 2014, 2019). Following the pattern of increased TIC during interglacial periods, a pronounced maximum in TIC at 126 m c.d. in the Pestani data can also be ascribed to MIS 31 (Fig. 3). Below MIS 31, maxima of TIC in both successions can be ascribed to MIS 33 at 1.114–1.104 Ma (Wagner *et al.* 2019; Leicher *et al.* 2021). K intensities show more variations compared to TIC particularly during glacial periods and imply, along with TIC data, that glacial and interglacial periods over the last 1.15 Myr, back to MIS 34, are not completely recorded in the Pestani sediment succession (Fig. 3). TOC/TN ratios are low at both sites and indicate a predominant autochthonous origin of organic matter with slightly increased allochthonous input during interglacial periods since 1.15 Ma. Based on the overall high proportion of fine-grained sediments and similar amplitude of grain-size variations at both sites, relatively deep-water conditions prevailed also at the Pestani site since 1.15 Ma (cf. Wilke *et al.* 2020). However, the proportion of fine-grained material is higher at the DEEP site (Fig. 3). As the lake is mainly fed by karst aquifers with low suspension load, slightly coarser sediments at the Pestani site could derive from more intense current activity at the lateral basin floor (cf. Wagner *et al.* 2008, 2012a) that may have diminished sedimentation of fine-grained material.

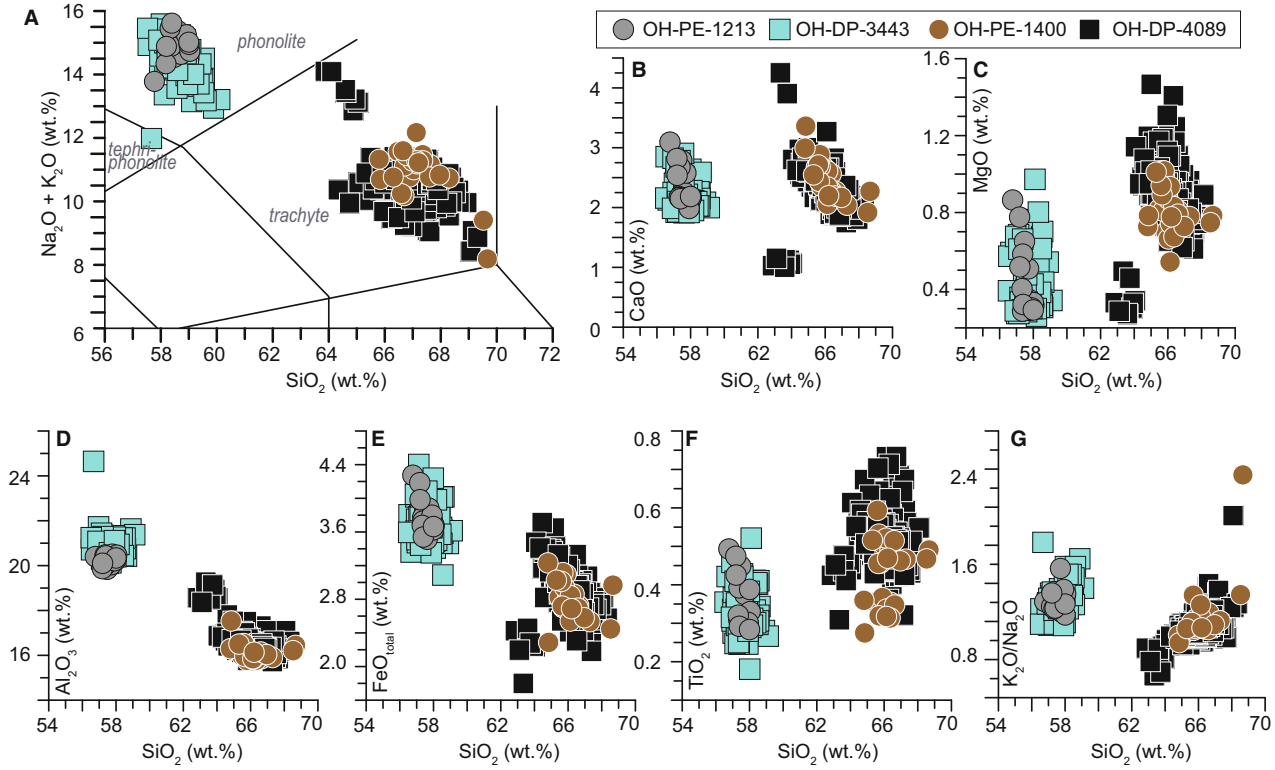

Fig. 4. TAS-diagram according to Le Bas *et al.* (1986) (A) and bioxide plots (B–G) of glass compositions of tephra layers OH-PE-1213/-1400 and OH-DP-3443/-4089 demonstrating the correlation of respective tephra layers from the Pestani and DEEP sites. Geochemical compositions of OH-DP-3443/-4089 are based on Leicher *et al.* (2021).

The stratigraphical correlation of the two sites over the last 1.15 Ma is supported by the geochemical correlation of 18 tephra layers (Tables 1, S1, Figs S1–S12), with tephra layers OH-DP-3443 and OH-PE-1213 deposited during MIS 27 being the lowermost tie points of this interval (Table 1, Figs 3, 4). Palaeomagnetic data also support the correlation. Although the occurrence of greigite distinctly distorts the palaeomagnetic data in some intervals, the base of the Matuyama–Brunhes reversal dated to 0.779 Ma and the base of the Jaramillo subchron dated to 1.072 Ma can clearly be identified in both records (Figs 3, 5; cf. Just *et al.* 2019). The latter is corroborated by distinct maxima in TIC and minima in K counts of MIS 31. Diatom assemblages from the DEEP site record show a clear dominance of planktonic taxa over the last 1.15 Ma and a preferred water depth range of 0–80 m (Fig. 6; cf. Wilke *et al.* 2020), except for the period around MIS 32, where a maximum of facultative planktonic taxa can be observed. The uppermost diatom sample from the Pestani site is from 126.88 m c.d., close to the base of the Jaramillo subchron (Fig. 3). As this sample does not contain *Pantocsekiella* sp. 2 nov, which has a pronounced maximum in the DEEP site sediment succession between 334 and 367 m c.d. (*c.* 0.956–1.052 Ma, Fig. 6), the age of this sample can be inferred to range between 1.052 Ma and the base of the Jaramillo subchron at 1.072 Ma (Fig. 3). Slightly downcore at both sites, a maximum in *Cyclotella sollevata* around 390 m c.d. in the DEEP site record corresponds with MIS 34 and with 132.3 m c.d. in the Pestani record. Although only four samples from the Pestani sediment succession cover the period between 1.052 and 1.15 Ma, they also show a maximum of facultative planktonic taxa (Fig. 6).

The stratigraphical correlation based on sedimentological data indicates that the Pestani sediment succession is mostly continuous back to 1.15 Ma. Periods that are disturbed or completely missing in the Pestani sediment succession include MIS 6–7, MIS 14 and MIS 28–29, which is supported by the GR data from borehole logging (Fig. 3; cf. Ulfers *et al.* 2022) and missing tephra layers (Table S1; Leicher *et al.* 2021). Hiatuses in the Pestani sediment succession at those times could originate from increased lake internal current activity, mass wasting, and/or tectonic activity. Increased lake internal current activity at the Pestani site is merely indicated by coarser sediments only for the periods around MIS 6 and MIS 14 (Fig. 3). Disrupted and tilted reflectors directly west of the Pestani site show tectonic activity and mass wasting, but this is not the case for reflectors that frame MIS 6–7, MIS 14 and MIS 28–29 (Fig. 2). However, the limited vertical resolution of seismic data of a few metres (Wagner *et al.* 2017) and the mismatch of sediment depth in the composite succession (m c.d.) and the real

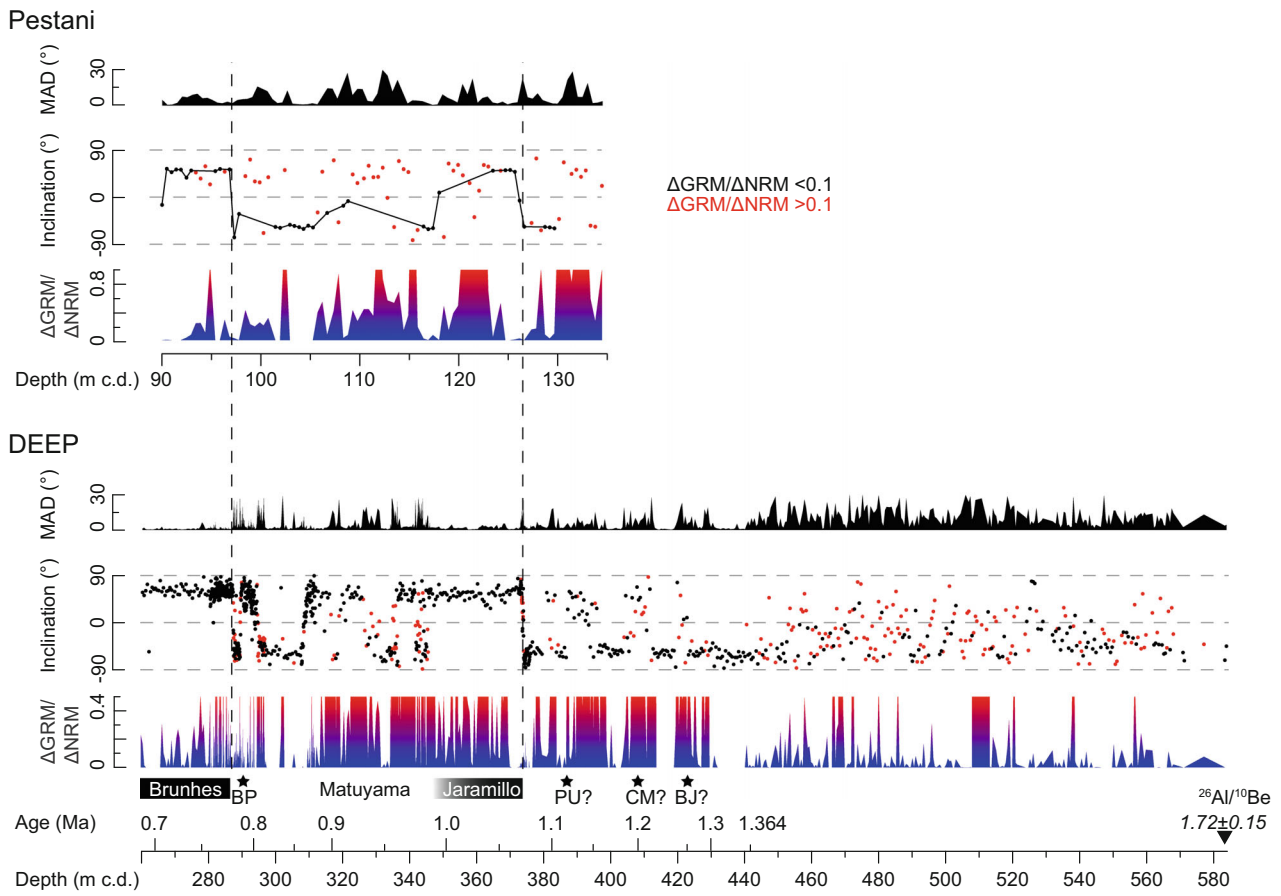

Fig. 5. Down-core magnetic parameters of the DEEP (bottom) and Pestani (top) sites vs. depth (m c.d.) and age at the DEEP site. DEEP site data down to 447 m c.d. are published in Just *et al.* (2019). Maximum angular deviation (MAD), inclination of the anchored characteristic remanent magnetization, and gyro-remanent magnetization vs. natural remanent magnetization (ΔGRM/ΔNRM), which reflects the impact of greigite on palaeomagnetic data, are shown according to Just *et al.* (2019). Inclinations of samples that acquired a significant GRM (ΔGRM/ΔNRM >10%) are shown in red. Vertical dashed lines provide correlation tie points between the DEEP and Pestani sediment successions at the Matuyama–Brunhes transition and at the base of the Jaramillo subchron. Geomagnetic excursions back to 1.36 Ma with the Brunhes precursor (BP), Punaruu (PU), Cobb Mountain (CM) and Bjorn (BJ) are according to Just *et al.* (2019). Also shown is the ^{26}Al/^{10}Be burial dating age from the base of the DEEP site sediment succession.

sediment depth (m b.l.f.) may bias the presumed ages of reflectors. During MIS 6 small mass wasting deposits likely contribute to an unusual sediment accumulation at the DEEP site (Fig. 3; cf. Francke *et al.* 2016) and also tephra layers at the Pestani site indicate some redeposition of sediments (Table S1). Hence, erosional mass wasting may have occurred during these periods, particularly if the Pestani site was located on a lake slope in former times. Although respective deposits are not found in the DEEP site sediment succession in substantial thickness, nor can be seen in the seismic data along the profile, they may occur to the north or south of the DEEP coring site.

Stratigraphical correlation beyond 1.15 Ma

For the stratigraphical correlation >1.15 Ma, we added data from palynological and stable isotope analyses, as this information is crucial to disentangle local from regional drivers of environmental variability. As the water in Lake Ohrid is well mixed and provides uniform lake water $\delta^{18}O$ ($\delta^{18}O_{LW}$), which is the primary control on $\delta^{18}O_C$ (Lacey *et al.* 2016), endogenic carbonate precipitated at DEEP or Pestani will have equivalent $\delta^{18}O_C$. In concert with other data, isotope data help to determine the environmental conditions during the onset of basin and lake formation and when a lacustrine environment connected the DEEP and Pestani sites.

The stratigraphical correlation between the DEEP and Pestani sites beyond 1.15 Ma (MIS 34) shows very similar fluctuations in TIC, K counts, TOC/TN ratio and grain-size data down to 408.9 m c.d. in the record from DEEP and 140.0 m c.d. from Pestani. At these depths, the occurrence of tephra layers OH-DP-4089 and OH-PE-1400 with similar major element geochemistry provides another independent tie point (Table 1, Fig. 4).

According to the chronology of the DEEP site record, tephra OH-DP-4089 was deposited during MIS 36 at *c.* 1.21 Ma (Leicher *et al.* 2021). The similarity of geochemical and grain-size variations between the DEEP and Pestani sites back to 1.21 Ma, including the relatively long-lasting MIS 35 around 1.16 Ma, implies that both sites were part of a larger lake rather than being located in separate basins. This is confirmed by diatom data, which show similar assemblage changes and relatively high abundances of planktonic taxa in the sediment successions from both sites (Fig. 6). More specifically, a maximum of *Stephanodiscus* sp. 1 nov at 406 m c.d. in the DEEP site record corresponds with a maximum during the middle of MIS 35 and 137 m c.d. in the Pestani record. Pollen assemblages from DEEP (400.6–406.646 m c.d.) and Pestani (133.5–138.3 m c.d.) corresponding to MIS 35 suggest a forested interval with *Abies*, *Cedrus* and *Tsuga* (maximum values at both sites) dominating at higher elevations, while mesophilous trees such as *Quercus*, *Carya*, *Carpinus* and riparian taxa such as *Liquidambar* (maximum values in both sites) occurred at lower elevations (Fig. 7). During MIS 36 (407.0–411.4 m c.d. in the DEEP site record) conifer (excluding *Pinus* and *Picea*) and mesophilous tree percentages decrease, whereas *Artemisia* and Poaceae increase, suggesting prevalence of cooler and drier climate conditions (e.g. Sadori *et al.* 2016; Koutsodendris *et al.* 2019). This corresponds with the interval 139.0–141.5 m c.d. in the Pestani record, but with higher mesophilous plant percentages in comparison to the DEEP site (Fig. 7).

Below tephra layers OH-DP-4089 and OH-PE-1400, or beyond MIS 36, a stratigraphical correlation of the DEEP and Pestani sediment records is more difficult. In addition to a potential match of TIC, K, TOC/TN ratio and grain-size data, a distinct decrease of *Pantocsekiella delicatula* and an increase of *Cyclotella sollevata* at 413 m c.d. in the DEEP site record suggest a correspondence with a similar shift at 142.6 m c.d. in the Pestani record (Figs 3, 6). $\delta^{13}C_C$ and $\delta^{18}O_C$ both increase at 414 m c.d. in the DEEP site record corresponding to an age of 1.23 Ma in MIS 37 (Wagner *et al.* 2019), which might correlate with a similar increase at 144.5 m c.d. in the Pestani record (Fig. 8). Pollen data support a correlation of the interval from 141.5 to 144.5 m c.d. in the Pestani record to the interval from 412.1 to 419.1 m c.d. in the DEEP site record (Fig. 7; Panagiotopoulos *et al.* 2020). During this interval, mesophilous and conifer taxa are co-dominant and conspicuous peaks of conifer species such as *Tsuga*, *Abies*, *Cedrus* occur in pollen spectra from both sites. Although the overall match of geochemical, grain-size, pollen and diatom data suggests that both sites were part of the same water body, some data suggest that the water depth at the DEEP site was substantially higher than at the Pestani site during that time. For example, planktonic diatom taxa with preferred water depths of up to 80 m predominate in the DEEP record, whilst a relatively high proportion of benthic or facultative planktonic taxa limited to 0–10 m water depths dominated the Pestani record during MIS 37 (Fig. 6). A shallower water depth at the Pestani site is reinforced by a more pronounced minimum in fine-grained (<16 μm) sediments and the occurrence of shell remains in the supposed MIS 37 interval of the Pestani record (Fig. 3).

Below MIS 37, a well-defined succession of the glacial and interglacial periods MIS 38–43 recorded at the DEEP site cannot be identified in the Pestani record (Fig. 3). Gaps in core recovery of up to several metres, distinct grain-size fluctuations, and the occurrence of shell remains in the Pestani sediment succession imply shallow and fluctuating water depths that led to discontinuous sediment accumulation. Therefore, a stratigraphical correlation of the two sites is restricted to individual sediment horizons that are characterized by specific changes in geochemical, pollen, diatom and isotope data. Based on the diatom data, a prominent minimum of *P. delicatula* at ~421 m c.d. might correspond to ~147 m c.d. in the Pestani record and would place this horizon within MIS 38 (Fig. 6). However, TIC and K values in this interval of the Pestani record are not typical of glacial conditions (Fig. 3). The record seems to be disturbed down to ~152 m c.d., where transitions in $\delta^{18}O_C$ and $\delta^{13}C_C$ correspond to similar transitions at ~432 m c.d. in the DEEP site record (Fig. 8). According to the DEEP chronology, these transitions are placed in MIS 41 (Fig. 3). Somewhat below, stable isotope data, particularly $\delta^{18}O_C$, show corresponding variations at ~440 m c.d. in the DEEP and at ~162 m c.d. in the Pestani record, which is supported by diatom data with increases of non-endemic planktonic *P. delicatula* and endemic benthic *Epithemia ohridana* (Fig. 6). Also pollen data support the correlation close to the onset of permanent lacustrine conditions at the DEEP site. Between 437.0 and 439.8 m c.d. in the DEEP site, relatively high herb percentages (up to 40%, mostly), similar mesophilous and conifer percentages, and maximum aquatic vascular plant percentages indicate glacial

Fig. 6. Shared endemic and non-endemic diatom taxa from the interval 300–510 m c.d. in the DEEP sediment succession and in interval 126–174 m c.d. in the Pestani sediment succession. DEEP site data down to 447 m c.d. are published in Panagiotopoulos *et al.* (2020), Wilke *et al.* (2020) and Jovanovska *et al.* (2022). Samples from 531, 543, 545, 548 and 551 m c.d. in the DEEP site sediment successions contained only a few diatoms and were not included here. Diatom-specific water-depth preferences are according to Panagiotopoulos *et al.* (2020). Tephrostratigraphical tie points OH-DP-4089 and OH-PE-1400 are marked in yellow, tie points based on shifts in diatom populations and/or assemblages are colour-coded according to Fig. 3. Taxa names in green represent taxa endemic to lakes Ohrid and Prespa, taxa names in blue are endemic to the Drim River only or both Lake Ohrid and Drim River (cf. Levkov & Williams 2012).

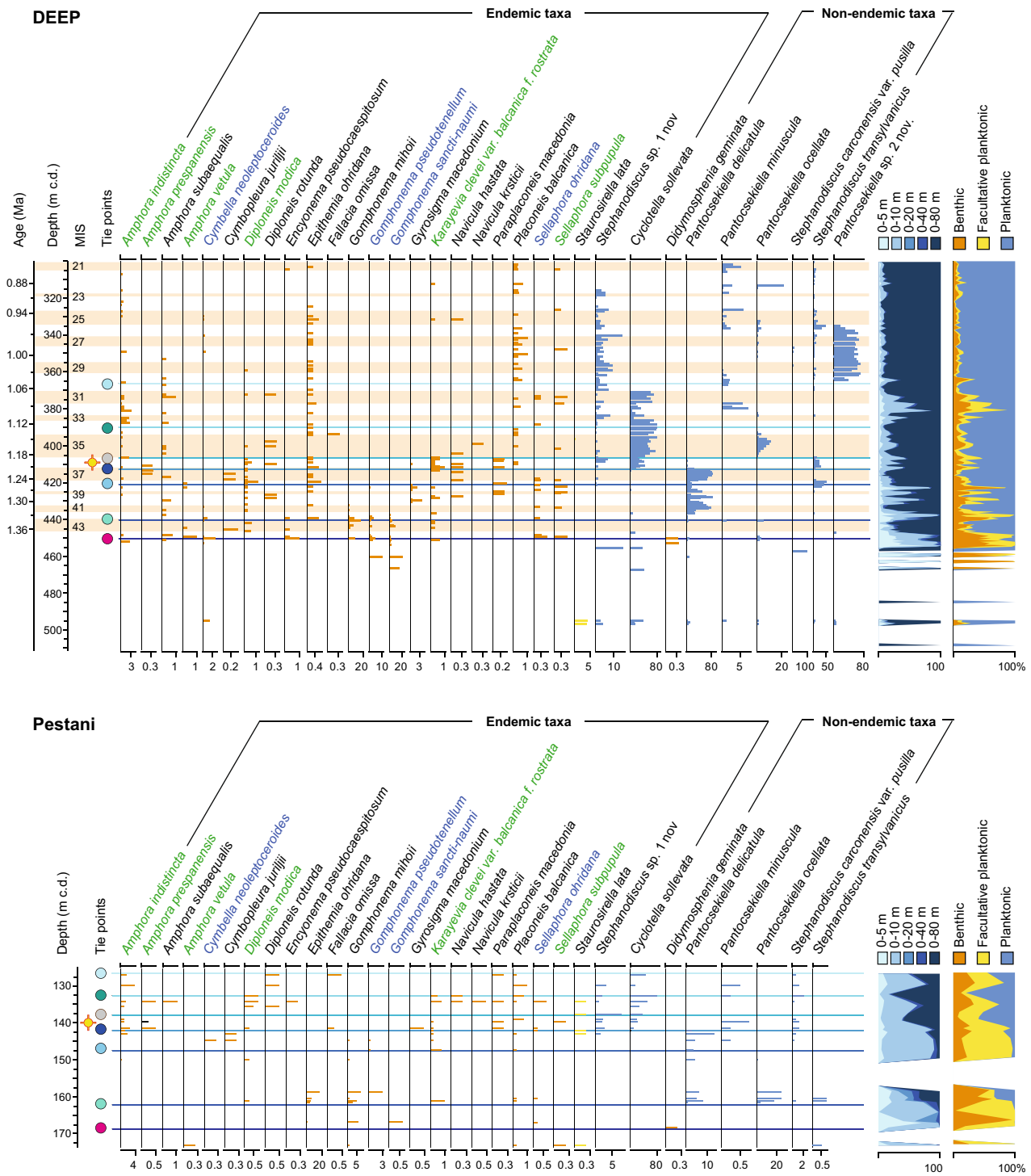

Tie points

	DEEP	Pestani	Characteristics
○	367 m c.d.	<126.88 m c.d.	First occurrence of *pantocsekiella* sp. 2
●	390 m c.d.	132.3 m c.d.	Peak of *C. sollevata*
○	406 m c.d.	137 m c.d.	Peak of *S.* sp. 1 nov
●	413 m c.d.	142.6 m c.d.	Decrease of *P. delicatula* and increase of *C. sollevata*
○	421 m c.d.	147 m c.d.	Minimum of *P. delicatula* below increase of *S.* sp. 1 nov
○	440 m c.d.	162 m c.d.	Increases of *P. delicatula* and *E. ohridana*
●	452 m c.d.	168 m c.d.	Occurrence of *D. geminata*

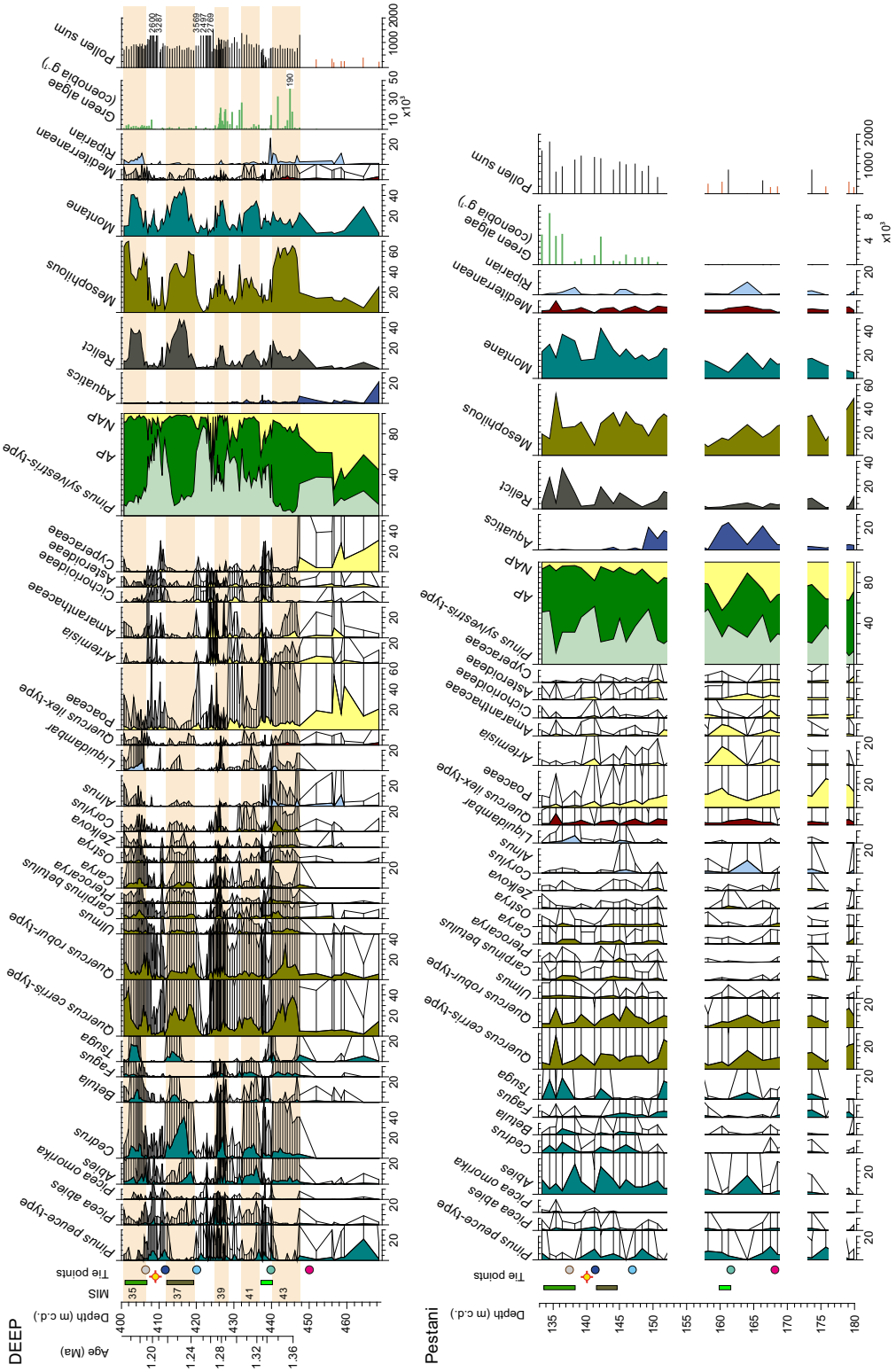

Fig. 7. Pollen percentage diagrams of selected (>2%) taxa (with ×10 exaggeration) from the interval 400–468 m c.d. from the DEEP sediment succession and from the interval 133–180 m c.d. from the Pestani sediment succession. DEEP site data down to 447 m c.d. are published in Panagiotopoulos *et al.* (2020). Species are colour-coded as mesophilous (olive), montane (teal), Mediterranean (dark red), riparian (blue) and herbs (yellow) according to Panagiotopoulos *et al.* (2020). Tie points include tephra layers OH-DP-4089 and OH-PE-1400 (yellow), shifts in diatom assemblages (colour-coded; Figs 3, 6) and specific palynological horizons marked by green rectangles (shading correlates between cores).

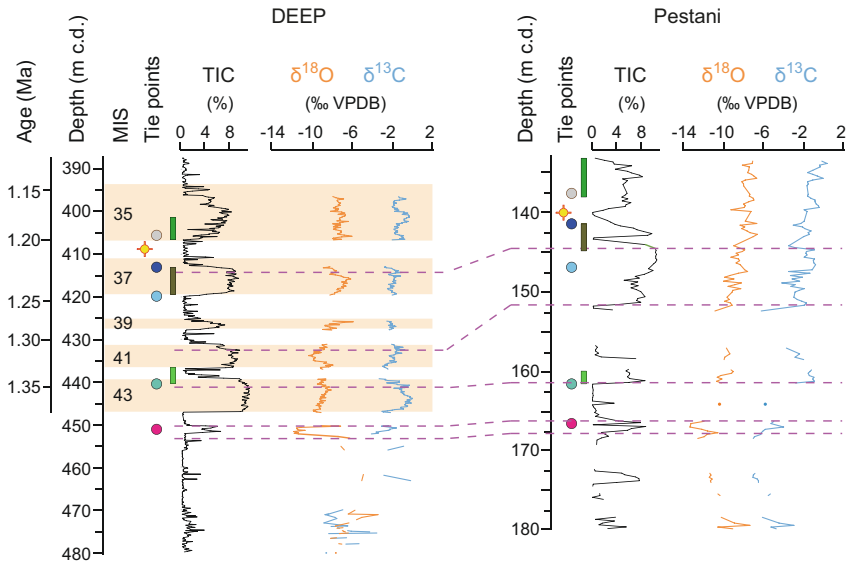

Fig. 8. Comparison of bulk carbonate oxygen and carbon isotopes ($\delta^{18}O_C$, $\delta^{13}C_C$) from the interval 385–480 m c.d. from the DEEP sediment succession and the interval 133–180 m c.d. from the Pestani sediment succession. DEEP site data down to 447 m c.d. are published in Wagner *et al.* (2019), Panagiotopoulos *et al.* (2020) and Wilke *et al.* (2020). Tie points include tephra layers OH-DP-4089 and OH-PE-1400 (yellow), shifts in diatom assemblages (colour-coded dots) and palynological correlations (colour-coded rectangles; Figs 3, 6, 7). Dashed purple lines indicate tie points from specific horizons with prominent shifts in bulk carbonate oxygen and carbon isotopes.

conditions of MIS 42. MIS 43 (440.2–447.3 m c.d.) is characterized by arboreal percentages above 80% with mesophilous species such as *Quercus* dominating and relatively low percentages of conifers. Pollen spectra from the Pestani site show relatively high percentages of Poaceae, Amaranthaceae and *Artemisia* between 160.1–161.5 m c.d. (Fig. 7), which can be tentatively correlated with MIS 42. Below this horizon, the sample resolution and pollen sum are too low for further down-core stratigraphical correlation between the two sites.

The existing age model of the DEEP site record ends at 447 m c.d., which corresponds to the transition between MIS 44 and MIS 43 at 1.364 Ma (Figs 3, 9). Slightly below this depth, at ~451 m c.d. in the DEEP site record, there is a pronounced minimum in $\delta^{18}O_C$ and a slight maximum in $\delta^{13}C_C$. The same pattern is found around 167 m c.d. in the Pestani record (Fig. 8). The similarity of the two records suggests that a water body already connected both sites prior to MIS 43. The stratigraphical correlation is supported by diatom data, which show a short occurrence of *Didymosphenia geminata* that is a widespread at these depths in both records, but very rare species in the Balkans (Fig. 6). Maxima in TIC and TOC/TN ratios and minima in K at these depths (Fig. 3) are typical for interglacial conditions and imply that the sediments were deposited during MIS 45. However, highly fluctuating grain sizes with a dominance of the coarse silt and sand fraction at both sites, in combination with peat horizons and the occurrence of shell remains at the DEEP site, indicate distinct changes in sedimentation characteristics, including fluvial or shallow water conditions or even desiccation and sediment redeposition. Shallow water conditions and/or increased proximity to the shore can also be inferred by high aquatic vascular plant and Poaceae percentages in the Pestani sediment succession below 160 m c.d. (Fig. 7).

Further stratigraphical correlation of proxies down-core is vague. Based on the sedimentation characteristics above, slight maxima in TIC at depths of around 462, 475, 490 and 500 m c.d. along with a higher proportion of fine-grained sediments at the DEEP site might correlate with similar horizons at 174, 180, 185 and 195 m c.d. in the Pestani record, respectively (Fig. 3). This is tentatively supported by a maximum in *Tsuga* pollen at 465 m c.d. in the sediment succession DEEP and at 174 m c.d. at Pestani (Fig. 7). However, the significantly lower pollen sums do not allow for reliable correlations and pollen samples from the DEEP site below 447 m c.d. and below 175 m c.d. from the Pestani site are most likely affected by the dynamic depositional environment.

Early basin and lake history

Chronological constraints of the early basin and lake

At the DEEP site, a tentative burial age from $^{26}Al/^{10}Be$ of 1.72±0.15 Ma (1 SE, n = 5) has been obtained for the lowermost core section from 586.18–585.64 m c.d. (Fig. 3, Table S2). Palaeomagnetic data from the DEEP sediment succession below the base of the Jaramillo subchron, in combination with the existing age model down to 447 m c.d. and 1.364 Ma, support this age estimation at the base of the succession. Three intervals of normal polarities at ~385, 409 and 423 m c.d. are

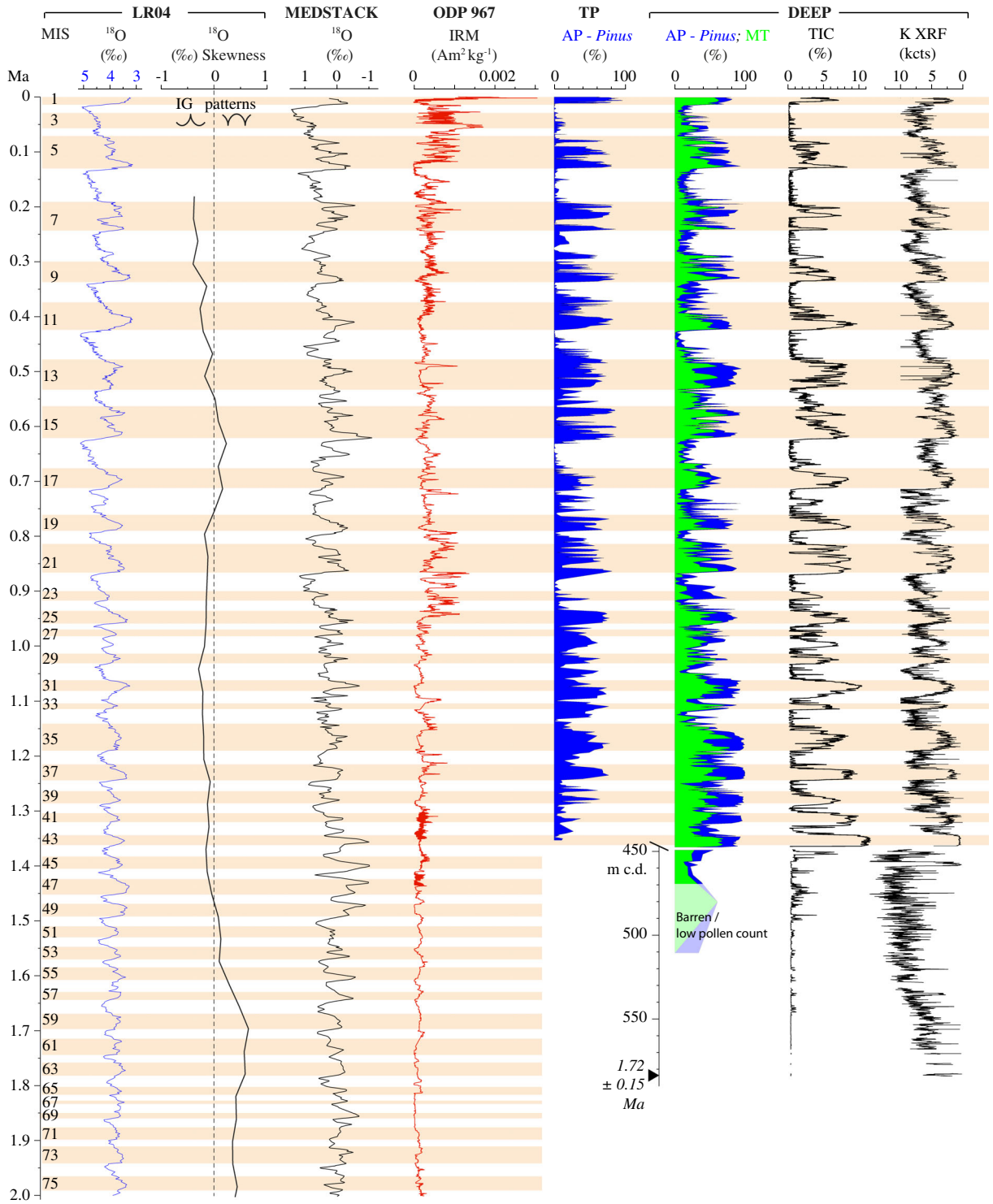

Fig. 9. Comparison of selected palaeoclimate records, including LR04 marine isotope stages (MIS) and global benthic $\delta^{18}O$ stack (Lisiecki & Raymo 2005), LR04 skewness showing a decrease in the relative duration of interglacials around 1.4 Ma (Lisiecki & Raymo 2007), stacked benthic $\delta^{18}O$ data for Ocean Drilling Program (ODP) sites 967 and 968 from the eastern Mediterranean (MEDSTACK; Wang *et al.* 2010), isothermal remanent magnetization (IRM) from ODP 967 as proxy for Saharan dust input (Grant *et al.* 2022), Tenaghi Philippon (TP) arboreal pollen (AP) excluding *Pinus*, *Betula* and *Juniperus*-type (Tzedakis *et al.* 2006; Donders *et al.* 2021 and references therein) DEEP site arboreal pollen (AP-*Pinus*) and mesophilous trees (MT; *Acer*, *Buxus*, *Carpinus betulus*, *Carya*, *Castanea*, *Celtis*, *Corylus*, *Fraxinus excelsior*/*oxycarpa*, *Hedera*, *Ostrya*/*Carpinus orientalis*, *Pterocarya*, *Q. cerris*-type, *Q. robur*-type, *Tilia*, *Ulmus*, *Zelkova*; cf. Donders *et al.* 2021) and geochemical data (total inorganic carbon (TIC) and potassium (K) kilocounts (kcts) from XRF scanning) vs. age back to 1.36 Ma and vs. metres composite depth (m c.d.) (Wagner *et al.* 2019; Panagiotopoulos *et al.* 2020; Donders *et al.* 2021) and complemented with new data (Figs 3, 7).

impacted by the potential occurrence of early diagenetic greigite and may record the Bjorn, Cobb Mountain, and Punaruu excursions (Fig. 5; Just *et al.* 2019). Greigite formation also biases the DEEP site palaeomagnetic data below 447 m c.d. The Gardar excursion dated to *c.* 1.46 Ma in records from the North Atlantic (Chanell 2017) cannot be identified in the DEEP sediment succession. Further downcore, at ~526 m c.d., ΔGRM/ΔNRM shows only a moderate imprint of greigite formation and a short normal polarity phase occurs, which could correlate with the Gilsa excursion dated to *c.* 1.55 Ma in records from the North Atlantic (Chanell 2017). However, MADs vary around 10° in this section of the DEEP core and make this correlation highly questionable (Figs 3, 5).

Seismic data from close to the DEEP site suggest that 120–130 m of presumably coarse-grained sediments were not recovered from below the deepest drill hole containing the oldest sediments in the basin (Fig. 3; Lindhorst *et al.* 2015). Extrapolation of the sedimentation rate (~3.9 m ka^{-1}) between 447 m c.d. (1.36 Ma) and 586 m c.d. (1.72±0.15 Ma) provides an estimate for the onset of sedimentation in the Lake Ohrid basin of ca. 2 Ma (Figs 3, 9), which supports earlier age estimations (cf. Wagner *et al.* 2014, 2017; Lindhorst *et al.* 2015). However, sedimentation rates may have varied significantly in a highly dynamic environment during the early graben formation and filling. The age estimations from the DEEP site suggest that TIC maxima below 447 m c.d. in the DEEP sediment succession are also related to interglacial periods (Figs 3, 9) and that an age of *c.* 1.5 Ma at ~500 m c.d. in the DEEP record can be tentatively transferred to the base of the Pestani record at ~195 m c.d. (Fig. 3). As seismic data suggest that the bedrock is ~5–15 m below the base of the recovered Pestani sediment succession, sedimentation here may have started not much earlier than 1.5 Ma.

Dynamic changes >1.4 Ma

Based on the seismic information and the sedimentological proxy data, the early basin was formed by a narrow, S to N trending valley (Lindhorst *et al.* 2015). Rounded cobbles and gravel at the base of the DEEP site sediment succession (Fig. 3; cf. Wagner *et al.* 2014) suggest that a fluvial system drained this valley shortly after its formation, at least around 1.72±0.15 Ma according to the burial age from $^{26}Al/^{10}Be$ dating. As the cobbles, gravel and sands are primarily composed of felsic silicates and siliciclastics, they likely originate from the Pliocene or Miocene conglomerates, sandstones and siltstones that are exposed today in the mountains to the southeast and southwest of Lake Ohrid (Hoffmann *et al.* 2010; Pashko & Aliaj 2020). Late Miocene to Quaternary coarse-grained sediments are also reported from outcrops and drill holes in the flat areas to the north of Lake Ohrid (Fig. 1; Dumurdzanov *et al.* 2004), but the seismic data from the SCOPSCO project do not support infill from this direction and show that the modern Lake Ohrid basin likely contains the oldest sediments in its central part (Wagner *et al.* 2014; Lindhorst *et al.* 2015). Thus, the coarse sediments at the base of the DEEP site sediment succession could have been transported by the (palaeo)river Drim, which is the outflow of Lake Ohrid today and may have had its source in the mountains south of Lake Ohrid at that time (Figs 1, 10). Overlying coarse-grained sediments are interspersed by more fine-grained sediments and peat layers, which indicates a highly variable and dynamic environment prior to *c.* 1.4 Ma. This early lake setting is supported by the diatom data showing that at the very beginning of lake formation, mixed assemblages with species endemic to the Drim springs (St. Naum; Figs 1, S13) and non-endemic taxa occurring in the surrounding rivers, prevailed (Fig. 6). Moreover, diatom data show slightly different successions at both sites. Diatoms occur only sporadically in the DEEP site record below 451 m c.d. that might correspond to MIS 45 (Figs 3, 6). At the Pestani site, diatoms have not been found below ~173 m c.d. The lack of corresponding diatom and stable isotope data below ~451 m c.d. in the DEEP site record and ~167 m c.d. in the Pestani record suggests that any ponds or small lakes that existed were likely separated from each other prior to *c.* 1.4 Ma (Fig. 3). At ~451 m c.d. in the DEEP site record and ~167 m c.d. in the Pestani record, i.e. probably during MIS 45, the very similar patterns of TIC, K, C/N ratio, grain size and isotope data, and a corresponding shift in diatom assemblages, suggest the presence of a first larger lake extending over the DEEP and Pestani sites. The higher aquatic vascular plant percentages at Pestani (20% at 150 m c.d.; Fig. 7) compared to the DEEP site suggest a rather distal location of the DEEP site to the shore in comparison with the Pestani site. However, this lake apparently persisted only for a short period or may have shifted its position as indicated by the incomplete records of both sides.

The $\delta^{18}O_C$ data from the base of the DEEP site record (below 452.08 m c.d.; Fig. 8) initially have an average $\delta^{18}O_C$ of −6.6‰ before lowering to an average of −11.4‰ between 451.92 and 450.32 m c.d. At the Pestani site, the base of the record (below 172.91 m c.d.) has average $\delta^{18}O_C$ of −10.3‰ decreasing to an average of −12.0‰ between 168.50 and 166.34 m c.d. (Fig. 8). This suggests that, prior to any continuous connection between the two sites, Pestani remained a through-flow dominated system (low $\delta^{18}O_C$) whereas the DEEP site may have been cut off from major inflows (Fig. 10), at least during drier months of the year, and underwent a degree of evaporation leading to higher $\delta^{18}O_C$. The Pestani site is located adjacent to springs that are part of the karst aquifer system that characterizes the Galičica Mountains to the east of the lake and is the main water tributary today. The Pestani site was likely groundwater-fed at this time and therefore the average

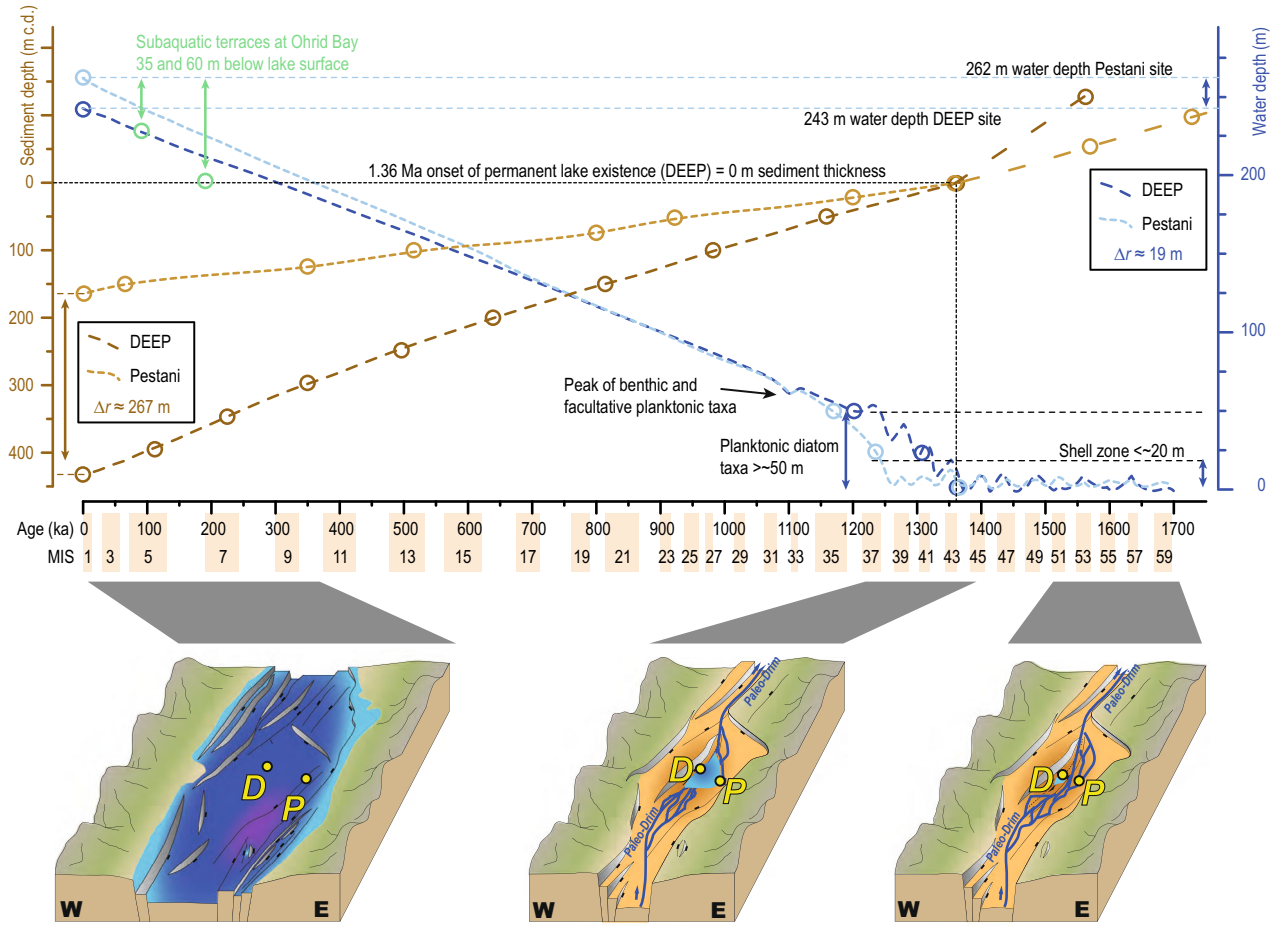

Fig. 10. Diagram showing the increase of reconstructed and recent water depths (right) from the DEEP (dark blue) and Pestani (light blue) sites. The difference in recent water depth between the two sites is 19 m. Reconstructed lake-level changes from former studies are indicated in greenish colour (left) and from Lindhorst *et al.* (2010). The increase in sediment thickness is based on the onset of permanent lacustrine conditions at the DEEP site at 1.36 Ma. Since then, 430 m (borehole logging data) of sediments have accumulated at the DEEP site (dark brown; ~447 m c.d. according to composite core, see Fig. 3) and ~163 m of sediment have accumulated at the Pestani site (light brown, ~165 m c.d. according to composite core, see Fig. 3). Sediment accumulation prior to 1.36 Ma is estimated and shown as negative values (left). The difference in recent sediment accumulation between the two sites is ~267 m. Ages and sediment depths of tie points (brownish dots) are taken according to Fig. 3. At the base, three cartoons modified from Lindhorst *et al.* (2015) show the environmental settings around *c.* 1.7 Ma, *c.* 1.4 Ma and in the Late Pleistocene (left to right).

$\delta^{18}O$ of inflow would have been low (average rainfall-fed spring inflows today have $\delta^{18}O = -10.1‰$; Lacey & Jones 2018). The shift in isotope data at both DEEP and Pestani to lower and similar $\delta^{18}O_C$ around MIS 45 marks a period of direct overlap between the two records (Fig. 8), supporting the presence of a larger body of water extending over the two sites (Fig. 10). In both records, the average $\delta^{18}O_C$ up to the lowermost chronological marker average −8.4 and −8.8 etc of isotope data between the two records during the continuous lacustrine conditions. The $\delta^{18}O_C$ increase of +3.0‰ at DEEP and +3.2‰ at Pestani is also constant between the two sites and suggests the increase in lake volume and residence time likely led to evaporation driving the higher $\delta^{18}O_{LW}$.

The settings of lakes Prespa and Ohrid during MIS 45 differed distinctly from the recent settings and a potential surface connection at that time has even been proposed (Stojadinović 1966). Increasing lake levels during MIS 45 could be the result of increased rainfall at that time, likely in combination with enhanced groundwater input to the lake potentially sourced from Lake Prespa (Fig. 1) and potentially supported by tectonic activation. Today, groundwater inflows account for over 50% of input to Lake Ohrid (Matzinger *et al.* 2007; Lacey & Jones 2018). Lake Prespa today is smaller than Lake Ohrid with significantly higher $\delta^{18}O_{LW}$ around −1.5‰. An enhanced groundwater connection between the sister lakes would increase the $\delta^{18}O$ of groundwater entering Lake Ohrid and could have led, in part, to the ~+3‰ shift in $\delta^{18}O_C$ observed in the DEEP and Pestani records. This would imply that Lake Prespa existed when Lake Ohrid started to fill, and Lake Ohrid may not be the oldest extant lake in Europe. This is in agreement with the formation of the Ohrid and Prespa basins during the

early Late Miocene (Pashko & Aliaj 2020), probably with slightly delayed formation of the Lake Ohrid basin during the latest Miocene (Burchfiel *et al.* 2008). Diatom data also indicate an early existence of Lake Prespa. During the formation of Lake Ohrid, species endemic to Lake Prespa or shared by lakes Prespa and Ohrid were among the first to establish in the developing waters of Lake Ohrid (together with non-endemic taxa originating mostly from the catchment and the surroundings; Fig. S13). More than half of the endemic diatom species are shared between the two lakes, supporting the connection of the two lakes in their early phase of existence. The lower number of endemic species, including across non-diatom taxa (e.g. Albrecht *et al.* 2012; Levkov & Williams 2012) could result from more pronounced lake-level fluctuations, increasing eutrophication (e.g. Matzinger *et al.* 2007; Wagner *et al.* 2012a), or discontinuous existence of Lake Prespa since that time. The latter possibility, however, is contradictory to the presence of highly specific diatom species, such as *Surirella rotunda*, *S. lineopunctata* and *S. imbuta*, within the contemporary endemic flora of Lake Ohrid, known as endemic for the contemporary flora of Lake Ohrid (Cvetkoska *et al.* 2014).

Stabilizing lacustrine conditions after 1.4 Ma

The DEEP site has been covered continuously by water since MIS 43 or 1.36 Ma (Wagner *et al.* 2019). In MIS 43 the proportion of planktonic diatom taxa with preferred water depth ranges of up to 80 m substantially increased at the DEEP site (Fig. 6). At the Pestani site, the first substantial increase in planktonic diatom taxa is slightly later, probably at the end of MIS 43, and with a higher proportion of taxa preferring water depths of <40 m (Figs 3, 6). As the early lacustrine history of Lake Ohrid and its catchment between MIS 43 and MIS 35 has been discussed already in detail based on data from the DEEP site (Panagiotopoulos *et al.* 2020), the focus here is on the comparison to the new data from the Pestani site. After 1.36 Ma and until *c.* 1.03 Ma (360 m c.d.), glacial periods at the DEEP site are characterized by a higher, but decreasing proportion of facultative planktonic or benthic taxa with preferred water depths of <10 m. Interglacial periods are characterized by higher rainfall (Wagner *et al.* 2019) and show a clear dominance of planktonic diatom taxa with preferred water depth ranges of up to 80 m. Indication of increasing water depths over time at both sites also comes from shell remains, which have a topmost occurrence in the DEEP sediment succession at ~435 m c.d. or during MIS 41 (Fig. 3). Today, the 'shell zone', where reworked shells accumulate, is reported at 10–30 m water depth (Albrecht & Wilke 2008; Cvetkoska *et al.* 2018). This zone likely was somewhat lower during the early phase of the lake, when the smaller lake size restricted wind fetch and wave activity. The topmost occurrence of shell remains in the DEEP sediment succession during MIS 41 (Fig. 3) along with the high proportion of planktonic and facultative planktonic diatom taxa in most samples above (Fig. 6) indicate that the water depth may have passed a treshold of 10-20 m at the DEEP site since that time (Fig. 10). This is supported by the shift to higher $\delta^{18}O_C$ indicating increased surface area and enhanced lake water evaporation. In addition, green algae comprising *Botryococcus* sp. and *Pediastrum* sp. are present in significant abundances in the DEEP site sediment succession between 1.36 and 1.26 Ma (Fig. 7) and point to the prevalence of shallow water conditions during this phase. In contrast, the lower abundance of green algae after 1.26 Ma indicates a shift to deeper and/or more oligotrophic water conditions at the DEEP site. This aligns well with climate change at the onset of the Mid-Pleistocene climate transition (cf. Panagiotopoulos *et al.* 2020) and likely was amplified around 1.15 Ma according to diatom data (Wilke *et al.* 2020).

In the Pestani record, low amounts of green algae below 150 m c.d. are consistent with the presence of a through-flow dominated system at this site prior to *c.* 1.26 Ma (Fig. 7). High green algae concentrations between 150 and 133 m c.d. suggest a connection between the Pestani and the DEEP sites and more stagnant and shallow water conditions. The topmost occurrence of shell remains in the Pestani record is at 145 m c.d. (Fig. 3). This implies that the water depth may not have exceeded the depth of the 'shell zone' at 10–30 m until MIS 37, i.e. much later than at the DEEP site (Fig. 10). It seems a larger lake extended over the Pestani and DEEP sites at least during interglacial periods, but with deeper waters at the DEEP site. During glacial periods, when rainfall was lower (Wagner *et al.* 2019), lake-level decrease might have affected particularly the Pestani site with its more lateral position in the lake and with increasing elevation relative to the DEEP site due to ongoing subsidence. This may explain the larger hiatuses in the core recovery and more disturbed sedimentation at the Pestani site until MIS 36 or *c.* 1.21 Ma. For that time, the Pestani record shows the first persistent occurrence of planktonic diatom taxa with preferred water depth ranges of up to 80 m. This increase in water depth explains why the Pestani record consists predominantly of fine-grained sediments and shows almost continuous sedimentation after *c.* 1.21 Ma. Seismic data confirm the first uninterrupted correlation of the DEEP and Pestani sites in MIS 36 (Fig. 2). However, the proportion of facultative planktonic and benthic taxa is higher in the Pestani record compared to the DEEP site record until 1.08 Ma. This is likely due to a slightly lower water depth compared to the same period in the DEEP site record. This may additionally be affected by the more lateral location of the Pestani site and thus a higher influence of shallower habitats. Although the diatom data imply a highly dynamic environment with overall increasing, but fluctuating water depth until *c.* 1.03 Ma, absolute values

of water depth are difficult to infer. The calculation of the preferred water depth is based on recent environmental settings. According to Secchi transparency measurements over recent decades, the upper 80 m of the water column comprises the entire photic zone. However, this zone might have been around 50 m or less in a shallower and potentially more trophic early lake phase (Fig. 10). More eutrophic conditions during this phase are indicated by relatively high proportions of eutrophic diatoms and green algae (Fig. 7; Panagiotopoulos *et al.* 2020; Wilke *et al.* 2020; Cvetkoska *et al.* 2021; Jovanovska *et al.* 2022). Above 360 m c.d. in the DEEP sediment succession, corresponding with *c.* 1.03 Ma, a clear dominance of planktonic taxa indicates further deepening and broadening of the lake such that larger parts of the central lake became part of the aphotic zone, where the water depth may have exceeded 40–80 m. From the Pestani site, the diatom record from the last 1.03 Ma has not been studied so far.

The morphology of the young and relatively narrow Lake Ohrid basin also may have influenced the surrounding vegetation. The distance between the DEEP and Pestani sites during the early lake phase likely was lower than today (Fig. 10). Wetland taxa, such as *Carya* or *Alnus*, may have been more abundant in flatter areas to the north or south. Higher percentages of Mediterranean taxa in Pestani (up to 10%, Fig. 7) could be associated with the presence of thermophilous vegetation near the coring location, while in DEEP show maximum values of 5%. Modern vegetation studies across the Galičica Mountains (Fig. 1) document the existence of thermophilous forests in the lowlands (Matevski *et al.* 2011). These findings point to a more local vegetation signal of the Pestani pollen record associated with the location of the coring site. This changed with ongoing lake broadening and the Pestani pollen record appears to capture a more regional vegetation signal upcore (from 150 m c.d.) recording two glacial–interglacial cycles corresponding to MIS 38–35. Despite the lower sample resolution of the Pestani record, the vegetational succession of individual taxa and the ecogroup trends (e.g. mesophilous and montane) observed show a close affinity to the ones documented in the DEEP record (Fig. 7).

Climatic implications

The climate significance of the DEEP site data covering the period of continuous existence of Lake Ohrid since 1.36 Ma has been highlighted in a number of papers (e.g. Wagner *et al.* 2019, Panagiotopoulos *et al.* 2020, Donders *et al.* 2021; Fig. 9). They include climate and altitude related vegetation differences compared to the Tenaghi Philippon peat sequence recovered from the Philippi basin in Eastern Macedonia, Greece (Figs 1, 9; Tzedakis *et al.* 2006; Donders *et al.* 2021). The new data from the bottom of the DEEP site sediment succession and the Pestani site sediment succession does not provide much additional information on palaeoclimate dynamics, as both sites show a highly variable and dynamic environment prior to *c.* 1.4 Ma that is mainly triggered by local processes, which overprint the climate significance. The fine-grained sediments and peat layers deposited at the DEEP and Pestani sites prior to *c.* 1.4 Ma, in conjunction with slight maxima in TIC and stable isotope data, indicate that slack water conditions may have persisted during interglacial periods, when rainfall was likely higher (Wagner *et al.* 2019). Although the burial age from $^{26}Al/^{10}Be$ of 1.72±0.15 Ma for the lowermost part of the DEEP site sediment succession can be used to roughly infer the onset of sedimentation in the lake basin, more reliable age information from the lowermost parts of the DEEP and Pestani sediment successions would be needed for palaeoclimate significance between *c.* 2.0 and 1.36 Ma.

Despite these restrictions, it is noteworthy that the onset of permanent lacustrine conditions in Lake Ohrid around 1.4 Ma is contemporaneous with the age of the base of the Tenaghi Philippon peat sequence (Figs 1, 9; Tzedakis *et al.* 2006). The sediment successions from both basins imply relatively dynamic environmental conditions prior to 1.4 Ma and subsequently stabilizing conditions (cf. Tzedakis *et al.* 2006; Pross *et al.* 2015). Although both basins are part of the Southern Balkan Extensional Region (Dumurdzanov *et al.* 2005), they are located ~300 km apart, which makes a solely tectonically driven ontogenesis of Lake Ohrid unlikely. The published sedimentological and diatom data from after 1.36 Ma indicate that deepening and widening of early Lake Ohrid was not a linear process and may have been affected by the interplay between the climate change at the onset of the Mid-Pleistocene climate transition and ongoing basin subsidence (cf. Panagiotopoulos *et al.* 2020). The timing of lake formation around 1.36 Ma rather corresponds with a major global climate transition. MIS 43 is the last interglacial of a series of high-amplitude interglacials (MIS 49–43) in the Mediterranean Sea (Fig. 9; Wang *et al.* 2010). This timing also corresponds with a shift to increasing dust flux from the Sahara into the eastern Mediterranean Sea (Fig. 9; Grant *et al.* 2022). Moreover, at this time, a change in glacial dynamics is associated with a decrease in modulation sensitivity to obliquity and a decrease in the relative duration of interglacials (Fig. 9; Lisiecki & Raymo 2007). However, a decrease in the relative duration of interglacials might have lowered the water supply to Lake Ohrid, as the lake is supposed to have received higher amounts of rainfall during interglacial periods (Wagner *et al.* 2019). The latter is supported by the new data from the DEEP and Pestani sites, which indicate higher water levels during interglacial periods at the onset of lake formation (Fig. 10). Given the regional synchronicity between the onset of sedimentation in the two basins, regional forcing mechanisms for the

formation of Lake Ohrid and the peat record from the Phillipi basin need to be explored.

Tectonic implications

The new data from the DEEP and Pestani sediment successions provide a better understanding of the history of the lake or basin deepening related to tectonic uplift and subsidence, respectively, by reconstructing sediment thicknesses and lake-water depth over time. However, the latter is challenging has been previously based on seismic and hydro-acoustic data and the formation of subaquatic terraces (Lindhorst *et al*. 2010; Wagner *et al*. 2017). The most prominent of these terraces at ~35 and ~60 m below the present lake level likely formed during MIS 5 and early MIS 6, respectively (Fig. 10), when relatively dry climate conditions may have persisted (Wagner *et al*. 2019).

The two sediment successions provide only a few hints on past changes in water depth. Today, the water depths at the coring locations differ by 19 m, with 243-m water depth at the DEEP site and 262 m at the Pestani site (Fig. 10; Wagner *et al*. 2014). Back in time, at the onset of permanent lacustrine conditions at the DEEP site at 1.36 Ma, the data from the DEEP and Pestani sites suggest that a shallow lake connected the two sites, likely with somewhat deeper water at the DEEP site according to the diatom data. The sporadic connection of the two sites by a shallow lake at or even prior to 1.36 Ma requires similar altitudes, differing probably by <20 m (Fig. 10).

The reconstruction of sediment thicknesses over time is based on the transfer of chronological information based on correlation using proxy data from the DEEP and Pestani sites. Both sites indicate a relatively constant increase in sediment thicknesses over time (Fig. 10). The $^{26}Al/^{10}Be$ age from the DEEP site indicates that ~120 m of sediment (borehole logging data; Fig. 3) may have accumulated at this site between *c*. 1.72 and 1.36 Ma. A tentative stratigraphical correlation of TIC maxima from DEEP to Pestani (Fig. 3) indicates that ~30 m of sediment may have accumulated at the Pestani site between *c*. 1.5 and 1.36 Ma (Fig. 10). Around 1.36 Ma, both sites were at a similar altitude. Since 1.36 Ma, ~430 m of sediment has accumulated at the DEEP site, whilst only ~163 m has accumulated at the Pestani site according to the borehole logging data (Fig. 3). Taking the altitude of the lake surface today (693 m a.s.l.), the water depth of 243 m at the DEEP site and 262 m at the Pestani site ($\Delta r \approx 19$ m; Fig. 10), and the sediment accumulation of 430 and 163 m ($\Delta r \approx 267$ m; Fig. 10), respectively, the level of the MIS 43 onset at 1.36 Ma is at ~20 m a.s.l. at the DEEP site and at ~268 m a.s.l. at the Pestani site today, i.e. differing by ~248 m. Sediment compaction may have altered the altitude of these horizons in the respective sites. In the upper 240 m of the sediment succession from the DEEP site, the sediment compaction was relatively constant and averaged at 14% (Baumgarten *et al*. 2015). When applying this rate to the two sites and the respective sediment thicknesses, the altitude of the 1.36-Ma horizon would be at ~80 m a.s.l. at the DEEP site and at ~300 m a.s.l. at the Pestani site, i.e. differing by ~220 m. Assigning a fairly high uncertainty to a potential difference in altitude of up to 20 m at the onset of the record and sediment compaction in the course of ongoing sedimentation, the vertical displacement between the sites can be estimated to 200–250 m since 1.36 Ma. This would result in vertical displacement rates of 0.15–0.18 mm a^{-1} for the last 1.36 Ma, with changes based on relatively small amounts of sediment accumulation over a long time scale (Fig. 10).

Only few data with respect to tectonic uplift exist from the region for comparison. On a very recent scale, which allows only tentative comparison to the long-term sedimentological data from the DEEP and Pestani sites, geodetic measurements recorded an uplift rate of <1 mm a^{-1} at the city of Ohrid (Fig. 1) between July 2000 and February 2021 (http://geodesy.unr.edu/NGLStationPages/stations/ORID.sta). The vertical displacement rates of 0.15–0.18 mm a^{-1} for the last 1.36 Ma at Lake Ohrid are distinctly lower compared to earlier measurements of current uplift rates of the surrounding mountains of >5 mm a^{-1} (Lilienberg 1968). They better correspond with an estimated uplift rate of 1 mm a^{-1} since the Pleistocene for the Jablanica Mountain range directly northwest of Lake Ohrid (Fig. 1) and with uplift rates of <1 mm a^{-1} in Balkan regions further to the east (Ruszkiczay-Rüdiger *et al*. 2020 and references therein). The Internal Albanides comprising Korabi zone rocks that also compose the mountains southeast of Lake Ohrid are characterized by a fission-track based long-term exhumation rate of 0.16 mm a^{-1} since *c*. 20 Ma, with a pulse of exhumation at 1.2 mm a^{-1} between 6 and 4 Ma (Muceku *et al*. 2008; Pashko & Aliaj 2020).

Overall, the rate of vertical displacement between the DEEP and Pestani sites in Lake Ohrid over the last *c*. 1.36 Ma seems to be in broad agreement with the few existing data from the region. The rate of vertical displacement seems to be relatively constant over time, at least on a long-term scale, which implies that the reconstructed orbital scale water-level changes particularly at the onset of lake formation are mainly related to changes in rainfall between glacial and interglacial periods.

Conclusions

Seismic profiles and deep drilling of Lake Ohrid provide the first detailed view into the early lake and basin history of what is thought to be the oldest extant lake in Europe. For this purpose, the 584-m-long sediment succession (5045–1) from the central DEEP site was compared to the

197-m-long sediment succession (5045–4) from the Pestani site further to the east, where drilling ended close to the bedrock.

Burial age estimations based on $^{26}Al/^{10}Be$ dating of clasts from the base of the DEEP sediment succession provided an age of 1.72±0.15 Ma. As 100–120 m of sediments fill from below the base of the recovered sediment succession are recorded in seismic data from this site, extrapolation of sedimentation rates implies an onset of sedimentation in the modern Lake Ohrid basin as early as *c*. 2 Ma. A narrow, south to north trending valley supported fluvial and slack water conditions, peat formation or even complete desiccation and characterized the early central basin history. Based on a comparison of geophysical, sedimentological and micropalaeontological data from the DEEP and the Pestani sites the sedimentation at the latter site started around 1.5 Ma. Prior to 1.36 Ma, the sediment successions from both sites indicate a highly dynamic environment in space and time. At 1.36 Ma the DEEP and Pestani sites were first connected in a joint lake basin, with slightly greater water depth at the DEEP site. Early Lake Ohrid underwent distinct lake-level fluctuations, with greater water depth in interglacial periods and gradual but fluctuating deepening and widening. The Pestani site indicates a more lateral location with more thermophilous vegetation in the vicinity and with shallower water conditions or desiccation particularly during glacial periods. A permanent larger lake has connected the two sites since 1.21 Ma.

There is no indication that a major tectonic event alone caused the formation of Lake Ohrid. Sediment accumulation rates imply a relatively constant vertical displacement by tectonic uplift and subsidence of ~0.2 mm a^{-1} between the central and the eastern lateral part of Lake Ohrid. Isotope and diatom data suggest that the filling of the Lake Ohrid basin partly originates from the (palaeo) river Drim, supported by the activation of the karst aquifer system at the eastern shore of Lake Ohrid. The data imply that Lake Prespa already existed when Lake Ohrid formed. The onset of ontogenesis of Lake Ohrid around 1.36 Ma is contemporaneous with the base of the Tenaghi Philippon pollen record and a major shift in global climate, when a decrease in the relative duration and amplitude of interglacial periods is proposed. As this indicates that the formation of Lake Ohrid is not solely driven by tectonic activity, the regional climate forcing needs to be explored in respect to higher amounts of precipitation, evapotranspiration and water supply during interglacial periods.

Acknowledgements. – This paper is dedicated to Andon Grazhdani, one of our co-authors, who passed away in May 2022. Andon Grazhdani substantially supported the Scientific Collaboration on Past Speciation Conditions in Lake Ohrid (SCOPSCO) drilling project since the presite surveys. It was a great honour to work with him. The SCOPSCO project and the presite surveys were funded by the International Continental Scientific Drilling Program (ICDP), the German Ministry of Higher Education and Research, the German Research Foundation, the University of Cologne, the British Geological Survey, the INGV and CNR (both Italy), and the governments of the republics of North Macedonia and Albania. S. Trajanovski and G. Kostoski from the Hydrobiological Institute in Ohrid and M. Sanxhaku and B. Lushaj from the Hydrometeorological Institute in Tirana provided logistic support for site surveys and the scientific drilling campaign. Drilling, Observation and Sampling of the Earth's Continental Crust (DOSECC) carried out the drilling. A. Skinner provided logistic and coordination support. We also thank the editor and the reviewers, Julie Brigham-Grette and an anonymous reviewer, for valuable comments and suggestions that helped to improve the manuscript. Open Access funding enabled and organized by Projekt DEAL. WOA Institution: UNIVERSITAET ZU KOLN Consortia Name: Projekt DEAL.

Author contributions. – Conceptualization by BW, PT, AF, NL; data acquisition by PT, AF, NL, SB, AC, EJ, JJ, JHL, ZL, KL, KK, SK, KP, AU, DZ, THD, AK, MS, TWo; project administration and funding acquisition by BW, ZL, AG, MJL, TWo, GZ, TWi; discussion, interpretation, writing and visualization by all authors; project coordination by BW.

References

Albrecht, C. & Wilke, T. 2008: Ancient Lake Ohrid: biodiversity and evolution. *Hydrobiologia 615*, 103–140.

Albrecht, C., Hauffe, T., Schreiber, K. & Wilke, T. 2012: Mollusc biodiversity in a European ancient lake system: lakes Prespa and Mikri Prespa in the Balkans. *Hydrobiologia 682*, 47–59.

Baumgarten, H., Wonik, T., Tanner, D. C., Francke, A., Wagner, B., Zanchetta, G., Sulpizio, R., Giaccio, B. & Nomade, S. 2015: Age-depth model of the past 630 kyr for Lake Ohrid (FYROM/Albania) based on cyclostratigraphic analysis of downhole gamma ray data. *Biogeosciences 12*, 7453–7465.

Binnie, S. A., Dunai, T. J., Voronina, E., Goral, T., Heinze, S. & Dewald, A. 2015: Separation of Be and Al for AMS using single-step column chromatography. *Nuclear Instruments and Methods in Physics Research Section B: Beam Interactions with Materials and Atoms 361*, 397–401.

Blott, S. J. & Pye, K. 2001: GRADISTAT: a grain size distribution and statistics package for the analysis of unconsolidated sediments. *Earth Surface Processes and Landforms 26*, 1237–1248.

Brigham-Grette, J., Melles, M., Minyuk, P., Andreev, A., Tarasov, P., DeConto, R., Koenig, S., Nowaczyk, N., Wennrich, V., Rosén, P., Haltia, E., Cook, T., Gebhardt, C., Meyer-Jacob, C., Snyder, J. & Herzschuh, U. 2013: Pliocene warmth, polar amplification, and stepped Pleistocene cooling recorded in NE Arctic Russia. *Science 340*, 1421–1427.

Burchfiel, B. C., King, R. W., Todosov, A., Kotzev, V., Dumurdzanov, N., Serafimovski, T. & Nurce, B. 2006: GPS results for Macedonia and its importance for the tectonics of the Southern Balkan extensional regime. *Tectonophysics 413*, 239–248.

Burchfiel, B. C., Nakov, R., Dumurdzanov, N., Papanikolaou, D., Tzankov, T., Serafimovski, T., King, R. W., Kotsev, V., Todosov, A. & Nurce, B. 2008: Evolution and dynamics of the Cenozoic tectonics of the South Balkan extensional system. *Geosphere 4*, 919–938.

Channell, J. E. T. 2017: Magnetic excursions in the late Matuyama Chron (Olduvai to Matuyama-Brunhes boundary) from North Atlantic IODP sites. *Journal of Geophysical Research Solid Earth 122*, 773–789.

Cvetkoska, A., Jovanovska, E., Francke, A., Tofilovska, S., Vogel, H., Levkov, Z., Donders, T., Wagner, B. & Wagner-Cremer, F. 2016: Ecosystem regimes and responses in a coupled ancient lake system from MIS 5b to present: the diatom record of lakes Ohrid and Prespa. *Biogeosciences 13*, 3147–3162.

Cvetkoska, A., Jovanovska, E., Hauffe, T., Donders, T. H., Levkov, Z., Van de Waal, D. B., Reed, J., Francke, A., Vogel, H., Wilke, T., Wagner, B. & Wagner-Cremer, F. 2021: Drivers of phytoplankton community structure change with ecosystem ontogeny during the

quaternary. *Quaternary Science Reviews 265*, 107046, https://doi.org/10.1016/j.quascirev.2021.107046.
Cvetkoska, A., Levkov, Z., Reed, J. M. & Wagner, B. 2014: Late glacial to Holocene climate change and human impact in the Mediterranean: the last ca. 17 ka diatom record of Lake Prespa (Macedonia/Albania/Greece). *Palaeogeography, Palaeoclimatology, Palaeoecology 406*, 22–32.
Cvetkoska, A., Pavlov, A., Jovanovska, E., Tofilovska, S., Blanco, S., Ector, L., Wagner-Cremer, F. & Levkov, Z. 2018: Spatial patterns of diatom diversity and community structure in ancient Lake Ohrid. *Hydrobiologia 819*, 197–215.
Dewald, A., Heinze, S., Jolie, J., Zilges, A., Dunai, T., Rethemeyer, J., Melles, M., Staubwasser, M., Kuczewski, B., Richter, J., Radtke, U., von Blanckenburg, F. & Klein, M. 2013: CologneAMS, a dedicated center for accelerator mass spectrometry in Germany. *Nuclear Instruments and Methods in Physics Research Section B: Beam Interactions with Materials and Atoms 294*, 18–23.
Donders, T. H., Panagiotopoulos, K., Koutsodendris, A., Bertini, A., Mercuri, A. M., Masi, A., Combourieu-Nebout, N., Joannin, S., Kouli, K., Kousis, I., Peyron, O., Torri, P., Florenzano, A., Francke, A., Wagner, B. & Sadori, L. 2021: 1.36 million years of Mediterranean forest refugium dynamics in response to glacial-interglacial cycle strength. *Proceedings of the National Academy of Sciences 118*, e2026111118, https://doi.org/10.1073/pnas.2026111118.
Dumurdzanov, N., Serafimovski, T. & Burchfiel, B. C. 2004: Evolution of the Neogene-Pleistocene basins of Macedonia. *Geological Society of America Digital Map and Chart Series 1*. Skopje, 2004.
Dumurdzanov, N., Serafimovski, T. & Burchfiel, B. C. 2005: Cenozoic tectonics of Macedonia and its relation to the South Balkan extensional regime. *Geosphere 1*, 1–22.
Francke, A., Conze, R., Pierdominici, S. & Gorgas, T. 2017: Core correlation using Corelyzer, Corelator and the drilling information system. *In* Harms, U. (ed.): *Planning, Managing, and Executing Continental Scientific Drilling Projects*, 93–101. GFZ German Research Centre for Geosciences, Potsdam.
Francke, A., Wagner, B., Just, J., Leicher, N., Gromig, R., Baumgarten, H., Vogel, H., Lacey, J. H., Sadori, L., Wonik, T., Leng, M. J., Zanchetta, G., Sulpizio, R. & Giaccio, B. 2016: Sedimentological processes and environmental variability at Lake Ohrid (Macedonia, Albania) between 640 ka and modern days. *Biogeosciences 13*, 1179–1196.
Granger, D. E. & Muzikar, P. F. 2001: Dating sediment burial with in situ-produced cosmogenic nuclides: theory, techniques, and limitations. *Earth and Planetary Science Letters 188*, 269–281.
Grant, K. M., Amarathunga, U., Amies, J. D., Hu, P. X., Qian, Y., Penny, T., Rodríguez-Sanz, L., Zhao, X., Heslop, D., Liebrand, D., Hennekam, R., Westerhold, T., Gilmore, S., Lourens, L. J., Roberts, A. P. & Rohling, E. J. 2022: Organic carbon burial in Mediterranean sapropels intensified during green Sahara periods since 3.2 Myr ago. *Nature Communications Earth and Environment 3*, 30, https://doi.org/10.1038/s43247-022-00357-1.
Hoffmann, N., Reicherter, K., Fernández-Steeger, T. & Grützner, C. 2010: Evolution of ancient Lake Ohrid: a tectonic perspective. *Biogeosciences 7*, 3377–3386.
Jovanovska, E., Cvetkoska, A., Hauffe, T., Levkov, Z., Wagner, B., Sulpizio, R., Francke, A., Albrecht, A. & Wilke, T. 2016: Differential resilience of ancient sister lakes Ohrid and Prespa to environmental disturbances during the late Pleistocene. *Biogeosciences 13*, 1149–1161.
Jovanovska, E., Hauffe, T., Stelbrink, B., Cvetkoska, A., Levkov, Z., Wagner, B., Lacey, J. H., Ognjanova-Rumenova, N., Hamilton, P. B., Brandenburg, K., Albrecht, C. & Wilke, T. 2022: Environmental filtering drives assembly of diatom communities over evolutionary timescales. *Global Ecology and Biogeography 31*, 954–967.
Just, J., Nowaczyk, N., Sagnotti, L., Francke, A., Vogel, H., Lacey, J. H. & Wagner, B. 2016: Climatic control on the occurrence of high-coercivity magnetic minerals and preservation of greigite in a 640 ka sediment sequence from Lake Ohrid (Balkans). *Biogeosciences 13*, 1179–1196.
Just, J., Sagnotti, L., Nowaczyk, N., Francke, A. & Wagner, B. 2019: Recordings of fast paleomagnetic reversals in a 1.2 ma greigite rich sediment archive from Lake Ohrid, Balkans. *Journal of Geophysical Research 124*, 12445–12464.
Kashiwaya, K., Ochiai, S., Sakai, H. & Kawai, T. 2001: Orbit-related long-term climate cycles revealed in a 12-Myr continental record from Lake Baikal. *Nature 410*, 71–74.
Kohl, C. P. & Nishiizumi, K. 1992: Chemical isolation of quartz for measurement of in situ-produced cosmogenic nuclides. *Geochimica et Cosmochimica Acta 56*, 3583–3587.
Kousis, I., Koutsodendris, A., Peyron, O., Leicher, N., Francke, A., Wagner, B., Giaccio, B., Knipping, M. & Pross, J. 2018: Centennial-scale vegetation dynamics and climate variability in SE Europe during marine isotope stage 11 based on a pollen record from Lake Ohrid. *Quaternary Science Reviews 190*, 20–38.
Koutsodendris, A., Kousis, I., Peyron, O., Wagner, B. & Pross, J. 2019: The marine isotope stage 12 pollen record from Lake Ohrid (SE Europe): investigating short-term climate change under extreme glacial conditions. *Quaternary Science Reviews 221*, 105873, https://doi.org/10.1016/j.quascirev.2019.105873.
Krastel, S., Leicher, N. & Harms, U. 2017: Pre-site survey and drill site selection for lake sediment coring. *In* Harms, U. (ed.): *ICDP Primer - Best Practices for Planning, Managing, and Executing Continental Scientific Drilling Projects*, 17–24. International Continental Scientific Drilling Program, Potsdam.
Lacey, J. H. & Jones, M. D. 2018: Quantitative reconstruction of early Holocene and last glacial climate on the Balkan Peninsula using coupled hydrological and isotope mass balance modelling. *Quaternary Science Reviews 202*, 109–121.
Lacey, J., Francke, A., Leng, M. J., Vane, C. H. & Wagner, B. 2015: A high resolution late glacial to Holocene record of environmental change in the Mediterranean from Lake Ohrid (Macedonia/Albania). *International Journal of Earth Sciences 104*, 1623–1638.
Lacey, J. H., Leng, M. J., Francke, A., Sloane, H. J., Milodowski, A., Vogel, H., Baumgarten, H. & Wagner, B. 2016: Mediterranean climate since the middle Pleistocene: a 640 ka stable isotope record from Lake Ohrid (Albania/Macedonia). *Biogeosciences 13*, 1801–1820.
Le Bas, M. J. L., Maitre, R. W. L., Streckeisen, A. & Zanettin, B. 1986: A chemical classification of volcanic rocks based on the Total alkali-silica diagram. *Journal of Petrology 27*, 745–750.
Lehmann, M. F., Bernasconi, S. M., Barbieri, A. & McKenzie, J. A. 2002: Preservation of organic matter and alteration of its carbon and nitrogen isotope composition during simulated and in situ early sedimentary diagenesis. *Geochimica et Cosmochimica Acta 66*, 3576–3584.
Leicher, N. 2021: *EPMA-WDS settings for glass at University of Cologne - v1*. Interdisciplinary Earth Data Alliance (IEDA), https://doi.org/10.26022/IEDA/111986.
Leicher, N., Giaccio, B., Zanchetta, G., Sulpizio, R., Albert, P., Tomlinson, E., Lagos, M., Francke, A. & Wagner, B. 2021: Lake Ohrid's tephrochronological dataset reveals 1.36 ma of Mediterranean explosive volcanic activity. *Nature Scientific Data 8*, 231, https://doi.org/10.1038/s41597-021-01013-7.
Leicher, N., Giaccio, B., Zanchetta, G., Wagner, B., Francke, A., Palladino, D. M., Sulpizio, R., Albert, P. & Tomlinson, E. L. 2019: Central Mediterranean explosive volcanism and tephrochronology during the last 630 ka based on the sediment record from Lake Ohrid. *Quaternary Science Reviews 226*, 106021, https://doi.org/10.1016/j.quascirev.2019.106021.
Leicher, N., Zanchetta, G., Sulpizio, R., Giaccio, B., Nomade, S., Wagner, B. & Francke, A. 2016: First tephrostratigraphic results of the DEEP site record in Lake Ohrid, Macedonia. *Biogeosciences 13*, 2151–2178.
Levkov, Z. & Williams, D. M. 2012: Checklist of diatoms (Bacillariophyta) from Lake Ohrid and Lake Prespa (Macedonia), and their watersheds. *Phytotaxa 45*, 1–76.
Lilienberg, D. A. 1968: The main regularities in recent movements in the central parts of the Balkan peninsula (on the example of Macedonia). *Studia Geophysica et Geodaetica 12*, 163–178.
Lindhorst, K., Gruen, M., Krastel, S. & Schwenk, T. 2012: Hydroacoustic analysis of mass wasting deposits in Lake Ohrid (FYR Macedonia/Albania). *In* Yamada, Y., Kawamura, K., Ikehara, K., Ogawa, Y., Urgeles, R., Mosher, D., Chaytor, J. & Strasser, M. (eds.):

Submarine Mass Movements and their Consequences, 245–253. Springer, The Netherlands.
Lindhorst, K., Krastel, S., Reicherter, K., Stipp, M., Wagner, B. & Schwenk, T. 2015: Sedimentary and tectonic evolution of Lake Ohrid (Macedonia/Albania). *Basin Research 27*, 84–101.
Lindhorst, K., Vogel, H., Krastel, S., Wagner, B., Hilgers, A., Zander, A., Schwenk, T., Wessels, M. & Daut, G. 2010: Stratigraphic analysis of lake level fluctuations in Lake Ohrid: an integration of high resolution hydro-acoustic data and sediment cores. *Biogeosciences 7*, 3531–3548.
Lisiecki, L. E. & Raymo, M. E. 2005: A Pliocene-Pleistocene stack of 57 globally distributed benthic $\delta^{18}O$ records. *Paleoceanography 20*, PA1003, https://doi.org/10.1029/2004PA001071.
Lisiecki, L. E. & Raymo, M. E. 2007: Plio–Pleistocene climate evolution: trends and transitions in glacial cycle dynamics. *Quaternary Science Reviews 26*, 56–69.
López-Blanco, C., Tasevska, O., Kostoski, G., Wagner, B. & Wilke, T. 2020: Ancient civilizations already had an impact on cladoceran assemblages in Europe's oldest lake. *Palaeogeography, Palaeoclimatology, Palaeoecology 552*, 109734, https://doi.org/10.1016/j.palaeo.2020.109734.
Matevski, V., Čarni, A., Avramovski, O., Juvan, N., Kostadinovski, M., Košir, P., Marinšek, A., Paušič, A. & Šilc, U. 2011: *Forest Vegetation of the Galičica Mountain Range in Macedonia*. 200 pp. Biološki inštitut Jovana Hadžija, Ljubljana.
Matzinger, A., Schmid, M., Veljanoska-Sarafiloska, E., Patceva, S., Guseska, D., Wagner, B., Müller, B., Sturm, M. & Wüest, A. 2007: Eutrophication of ancient Lake Ohrid: global warming amplifies detrimental effects of increased nutrient inputs. *Limnology and Oceanography 52*, 338–353.
Meyers, P. A. & Ishiwatari, R. 1995: Organic matter accumulation records in lake sediments. *In* Lerman, A., Imboden, D. M. & Gat, J. R. (eds.): *Physics and Chemistry of Lakes*, 279–328. Springer Verlag, Berlin.
Muceku, B., van der Beck, P., Bernet, M., Reiness, P., Masce, G. & Tashko, A. 2008: Thermochronological evidence for Mio-Pliocene late orogenic extension in the north-eastern Albanides (Albania). *Terra Nova 20*, 180–187.
Niessen, F., Gebhard, C. A., Kopsch, C. & Wagner, B. 2007: Seismic investigation of the El'gygytgyn crater Lake (central Chukotka, NE Siberia): preliminary results. *Journal of Paleolimnology 37*, 49–63.
Nishiizumi, K. 2004: Preparation of ^{26}Al AMS standards. *Nuclear Instruments and Methods in Physics Research Section B: Beam Interactions with Materials and Atoms 223*, 388–392.
Nishiizumi, K., Imamura, M., Caffee, M. W., Southon, J. R., Finkel, R. C. & McAninch, J. 2007: Absolute calibration of ^{10}Be AMS standards. *Nuclear Instruments and Methods in Physics Research Section B: Beam Interactions with Materials and Atoms 258*, 403–413.
Oberhänsli, H. & Molnar, P. 2012: Climate evolution in Central Asia during the past few million years: a case study from Issyk Kul. *Scientific Drilling 13*, 51–57.
Panagiotopoulos, K., Holtvoeth, J., Kouli, K., Marinova, E., Francke, A., Cvetkoska, A., Jovanovska, E., Lacey, J. H., Lyons, E. T., Buckel, C., Bertini, A., Donders, T. H., Just, J., Leicher, N., Leng, M. J., Melles, M., Pancost, R. D., Sadori, L., Tauber, P., Vogel, H., Wagner, B. & Wilke, T. 2020: Insights into the evolution of the young Lake Ohrid ecosystem and vegetation succession from a southern European refugium during the early Pleistocene. *Quaternary Science Reviews 227*, 106044, https://doi.org/10.1016/j.quascirev.2019.106044.
Pashko, P. & Aliaj, S. 2020: Stratigraphic and tectonic evolution of late Miocene–Quaternary basins in eastern Albania: a review. *Bulletin Geological Society of Greece 56*, 317–351.
Popovska, C. & Bonacci, O. 2007: Basic data on the hydrology of lakes Ohrid and Prespa. *Hydrological Processes 21*, 658–664.
Pross, J., Koutsodendris, A., Christanis, K., Fischer, T., Fletcher, W. J., Hardiman, M., Kalaitzidis, S., Knipping, M., Kotthoff, U., Milner, A. M., Müller, U. C., Schmiedl, G., Siavalas, G., Tzedakis, P. C. & Wulf, S. 2015: The 1.35-ma-long terrestrial climate archive of Tenaghi Philippon, northeastern Greece: evolution, exploration, and perspectives for future research. *Newsletters on Stratigraphy 48*, 253–276.
Reicherter, K., Hoffmann, N., Lindhorst, K., Krastel, S., Fernandez-Steeger, T., Grützner, C. & Wiatr, T. 2011: Active basins and neotectonics: Morphotectonics of the Lake Ohrid Basin (FYROM and Albania). *Zeitschrift der Deutschen Gesellschaft für Geowissenschaften 162*, 217–234.
Ruszkiczay-Rüdiger, Z., Kern, Z., Temovski, M., Madarász, B., Milevski, I., Braucher, R. & ASTER Team 2020: Last deglaciation in the Central Balkan Peninsula: geochronological evidence from the Jablanica mt. (North Macedonia). *Geomorphology 351*, 106985, https://doi.org/10.1016/j.geomorph.2019.106985.
Sadori, L., Koutsodendris, A., Panagiotopoulos, K., Masi, A., Bertini, A., Combourieu-Nebout, N., Francke, A., Kouli, K., Joannin, S., Mercuri, A. M., Peyron, O., Torri, P., Wagner, B., Zanchetta, G., Sinopoli, G. & Donders, T. H. 2016: Pollen-based paleoenvironmental and paleoclimatic change at Lake Ohrid (SE Europe) during the past 500 ka. *Biogeosciences 13*, 1423–1437.
Salzburger, W., Bocxlaer, B. V. & Cohen, A. S. 2014: Ecology and evolution of the African Great Lakes and their faunas. *Annual Review of Ecology, Evolution, and Systematics 45*, 519–545.
Scholz, C. A., Klitgord, K. D., Hutchinson, D. R., Ten Brink, U. S., Zonenshain, L. P., Golmshtok, A. Y. & Moore, T. C. 1993: Results of 1992 seismic reflection experiment in Lake Baikal. *Eos Transactions 74*, 465–470.
Stelbrink, B., Jovanovska, E., Levkov, Z., Ognjanova-Rumenova, N., Wilke, T. & Albrecht, C. 2018: Diatoms do radiate: evidence for a freshwater species flock. *Journal of Evolutionary Biology 31*, 1969–1975.
Stelbrink, B., Shirokaya, A. A., Föller, K., Wilke, T. & Albrecht, C. 2016: Origin and diversification of Lake Ohrid's endemic acroloxid limpets: the role of geography and ecology. *BMC Evolutionary Biology 16*, 273, https://doi.org/10.1186/s12862-016-0826-6.
Stojadinović, Č. 1966: Ein Rückblick auf die Resultate der bisherigen Forschungen der Becken der Dessaretischen Seen und die ehemaligen hydrographischen Verbindungen zwischen ihnen. *Revue Geographique 4*, 27–37.
Sušnik, S., Knizhin, I., Snoj, A. & Weiss, S. 2006: Genetic and morphological characterization of a Lake Ohrid endemic, *Salmo* (*Acantholingua*) *ohridanus* with a comparison to sympatric *Salmo trutta*. *Journal of Fish Biology 68* (A), 2–23.
Thomas, C., Francke, A., Vogel, H., Wagner, B. & Ariztegui, D. 2020: Weak influence of paleoenvironmental conditions on the subsurface biosphere of Lake Ohrid in the last 515 ka. *Microorganisms 8*, 1736, https://doi.org/10.3390/microorganisms8111736.
Trajanovski, S., Albrecht, C., Schreiber, K., Schultheiß, R., Stadler, T., Benke, M. & Wilke, T. 2010: Testing the spatial and temporal framework of speciation in an ancient lake species flock: the leech genus *Dina* (Hirudinea: Erpobdellidae) in Lake Ohrid. *Biogeosciences 7*, 3387–3402.
Tzedakis, P. C., Hooghiemstra, H. & Pälike, H. 2006: The last 1.35 million years at Tenaghi Philippon: revised chronostratigraphy and long-term vegetation trends. *Quaternary Science Reviews 25*, 3416–3430.
Ulfers, A., Zeeden, C., Wagner, B., Krastel, S., Buness, H. & Wonik, T. 2022: Borehole logging and seismic data from Lake Ohrid (North Macedonia/Albania) as a basis for age-depth modelling over the last one million years. *Quaternary Science Reviews 276*, 107295, https://doi.org/10.1016/j.quascirev.2021.107295.
Vogel, H., Wagner, B., Zanchetta, G., Sulpizio, R. & Rosén, P. 2010b: A paleoclimate record with tephrochronological age control for the last glacial-interglacial cycle from Lake Ohrid, Albania and Macedonia. *Journal of Paleolimnology 41*, 407–430.
Vogel, H., Wessels, M., Albrecht, C., Stich, H. B. & Wagner, B. 2010a: Spatial variability of recent sedimentation in Lake Ohrid (Albania/Macedonia). *Biogeosciences 7*, 3333–3342.
Wagner, B., Aufgebauer, A., Vogel, H., Zanchetta, G., Sulpizio, R. & Damaschke, M. 2012a: Late Pleistocene and Holocene contourite drift in Lake Prespa (Albania/F.Y.R. of Macedonia/Greece). *Quaternary International 274*, 112–121.
Wagner, B., Francke, A., Sulpizio, R., Zanchetta, G., Lindhorst, K., Krastel, S., Vogel, H., Rethemeyer, J., Daut, G., Grazhdani, A., Lushaj, B. & Trajanovski, S. 2012b: Possible earthquake trigger for 6^{th} century mass wasting deposit at Lake Ohrid (Macedonia/Albania). *Climate of the Past 8*, 2069–2078.

Wagner, B., Reicherter, K., Daut, G., Wessels, M., Matzinger, A., Schwalb, A., Spirkovski, Z. & Sanxhaku, M. 2008: The potential of Lake Ohrid for long-term palaeoenvironmental reconstructions. *Palaeogeography, Palaeoclimatology, Palaeoecology 259*, 341–356.

Wagner, B., Wilke, T., Krastel, S., Zanchetta, G., Sulpizio, R., Reicherter, K., Leng, M. J., Grazhdani, A., Trajanovski, T., Francke, A., Lindhorst, K., Levkov, Z., Cvetkoska, A., Reed, J., Zhang, X., Lacey, J., Wonik, T., Baumgarten, H. & Vogel, H. 2014: The SCOPSCO drilling project recovers more than 1.2 million history from Lake Ohrid. *Scientific Drilling 17*, 19–29.

Wagner, B. and 46 others 2017: The environmental and evolutionary history of Lake Ohrid (FYROM/Albania): interim results from the SCOPSCO deep drilling project. *Biogeosciences 14*, 2033–2054.

Wagner, B. and 47 others 2019: Mediterranean winter rainfall in phase with African monsoon during past 1.36 million years. *Nature 573*, 256–260.

Wang, P., Tian, J. & Lourens, L. J. 2010: Obscuring of long eccentricity cyclicity in Pleistocene oceanic carbon isotope records. *Earth and Planetary Science Letters 290*, 319–330.

Wilke, T., Wagner, B., Albrecht, C., Ariztegui, D., Van Bocxlaer, B., Delicado, D., Francke, A., Harzhauser, M., Hauffe, T., Holtvoeth, J., Just, J., Leng, M. J., Levkov, Z., Penkman, K., Sadori, L., Skinner, A., Stelbrink, B., Vogel, H., Wesselingh, F. & Wonik, T. 2016: Scientific drilling projects in ancient lakes: integrating geological and biological histories. *Global and Planetary Change 143*, 118–151.

Wilke, T. and 32 others 2020: Deep drilling reveals massive shifts in evolutionary dynamics after formation of ancient lake ecosystem. *Science Advances 6*, eabb2943, https://doi.org/10.1126/sciadv.abb2943.

Zanchetta, G., Baneschi, I., Francke, A., Boschi, C., Regattieri, E., Wagner, B., Lacey, J. H., Leng, M. J., Vogel, H. & Sadori, L. 2018: Evidence for carbon cycling in a large freshwater lake in the Balkans over the last 0.5 million years using the isotopic composition of bulk organic matter. *Quaternary Science Reviews 202*, 154–165.

Zaova, D., Cvetkoska, A., Wagner, B., Francke, A., Vogel, H., Levkov, Z. & Jovanovska, E. 2022: Diatom community responses to environmental change in Lake Ohrid (Balkan Peninsula) during the mid-Pleistocene transition. *Quaternary International 622*, 1–9.

Supporting Information

Additional Supporting Information to this article is available at http://www.boreas.dk.

Fig. S1. TAS-diagram (A) after Le Bas *et al*. (1986), CaO/FeO vs. Cl diagram (B) after Giaccio *et al*. (2019) and bioxide plots (C–K) of tephra equivalents OH-PE-0024/OH-DP-0015 and OH-PE-0017/OH-DP-0169. Geochemical data for tephra layers from the DEEP site are based on Leicher *et al*. (2021).

Fig. S2. TAS-diagram (A) after Le Bas *et al*. (1986), CaO/FeO vs. Cl diagram (B) after Giaccio *et al*. (2019) and bioxide plots (C–K) of tephra equivalents OH-PE-0208/OH-DP-0404, OH-PE-0214/OH-DP-0435 and OH-PE-0225/-0273.0/OH-DP-0624. Geochemical data for tephra layers from the DEEP site are based on Leicher *et al*. (2021).

Fig. S3. TAS-diagram (A) after Le Bas *et al*. (1986), pantellerite/comendite classification (B) after MacDonald (1974) and bioxide plots (C–K) of tephra equivalents OH-PE-0222/-0223/-0228 and OH-DP-0505/-0499. Geochemical data for tephra layers from the DEEP site are based on Leicher *et al*. (2021).

Fig. S4. TAS-diagram (A) after Le Bas *et al*. (1986), CaO/FeO vs. Cl diagram (B) after Giaccio *et al*. (2019) and bioxide plots (C–K) of tephra equivalents OH-PE-0273.9/OH-PE-0997 and OH-PE-0294.4/-0294.8/OH-DP-1175. OH-DP-1006 and OH-DP-1055 are also shown, but equivalents are not found in the Pestani succession. Geochemical data for tephra layers from the DEEP site are based on Leicher *et al*. (2021).

Fig. S5. TAS-diagram (A) after Le Bas *et al*. (1986), CaO/FeO vs. Cl diagram (B) after Giaccio *et al*. (2019) and bioxide plots (C–K) of tephra equivalents OH-PE-0402/OH-DP-1527. An equivalent of OH-PE-0306 was not identified in the DEEP site succession. Geochemical data for tephra layers from the DEEP site are based on Leicher *et al*. (2021).

Fig. S6. TAS-diagram (A) after Le Bas *et al*. (1986), CaO/FeO vs. Cl diagram (B) after Giaccio *et al*. (2019) and bioxide plots (C–K) of tephra equivalents OH-PE-0452/OH-DP-1640 and OH-PE-0565/OH-DP-1812. Geochemical data for tephra layers from the DEEP site are based on Leicher *et al*. (2021).

Fig. S7. TAS-diagram (A) after Le Bas *et al*. (1986), CaO/FeO vs. Cl diagram (B) after Giaccio *et al*. (2019) and bioxide plots (C–K) of tephra equivalents OH-PE-0569/OH-DP-1817. Geochemical data for tephra layers from the DEEP site are based on Leicher *et al*. (2021).

Fig. S8. TAS-diagram (A) after Le Bas *et al*. (1986), CaO/FeO vs. Cl diagram (B) after Giaccio *et al*. (2019) and bioxide plots (C–K) of tephra equivalents OH-PE-0600/OH-DP-1911, OH-PE-0616/OH-DP-1955 and OH-PE-0622/OH-DP-1966. Geochemical data for tephra layers from the DEEP site are based on Leicher *et al*. (2021).

Fig. S9. TAS-diagram (A) after Le Bas *et al*. (1986), CaO/FeO vs. Cl diagram (B) after Giaccio *et al*. (2019) and bioxide plots (C–K) of tephra equivalents OH-PE-0642/OH-DP-2010, OH-PE-0648/OH-DP-2017 and OH-PE-0801/OH-DP-2555. Geochemical data for tephra layers from the DEEP site are based on Leicher *et al*. (2021).

Fig. S10. TAS-diagram (A) after Le Bas *et al*. (1986), CaO/FeO vs. Cl diagram (B) after Giaccio *et al*. (2019) and bioxide plots (C–K) of tephra equivalents OH-PE-0819/OH-DP-2603 and OH-PE-0888/OH-DP-2669. No equivalent of OH-PE-0873 was identified in the DEEP site succession. Geochemical data for tephra layers from the DEEP site are based on Leicher *et al*. (2021).

Fig. S11. TAS-diagram (A) after Le Bas *et al*. (1986), CaO/FeO vs. Cl diagram (B) after Giaccio *et al*. (2019)

and bioxide plots (C–K) of tephra equivalents OH-PE-0965/OH-DP-2869 and OH-PE-0983/OH-DP-2898. Geochemical data for tephra layers from the DEEP site are based on Leicher *et al*. (2021).

Fig. S12. TAS-diagram (A) after Le Bas *et al*. (1986), CaO/FeO vs. Cl diagram (B) after Giaccio *et al*. (2019) and bioxide plots (C–K) of tephra equivalents OH-PE-1111/OH-DP-3144, OH-PE-1213/OH-DP-3443 and OH-PE-1400/OH-DP-4089.

Fig. S13. Variations in diatom relative abundances and accumulation of endemic diversity from the DEEP sediment succession over the last 1.36 Ma. (A) Diatoms characteristic for spring (teal bars) and river (olive bars) conditions, showing the relative abundance of taxa characteristic for St. Naum springs and the surrounding rivers today. *y* axis truncated at 30% and cut-off maxima values printed where applicable. (B) Species accumulation of endemic diatoms from Lake Ohrid (grey circles), Lake Prespa (light purple circles), lakes Ohrid and Prespa (dark purple circles) and St. Naum springs (green circles), listed according to time of occurrence in the DEEP sediment record. Vertical grey and white bars indicate glacial and interglacial periods, respectively.

Table S1. Tephra layers identified in the Pestani sediment succession and their equivalents from the DEEP site. Ages of DEEP site tephra derived from the age-model in Wagner *et al*. (2019). Correlated equivalents according to Leicher *et al*. (2016, 2019, 2021). ET = Etna, CF = Campi Flegrei; PA = Pantelleria; CVZ = Campanian Volcanic Zone; RMF = Roccamonfina; SVD = Sabatini Volcanic District; CA = Colli Albani.

Table S2. Cosmogenic nuclide analysis and results. The ^{10}Be and ^{26}Al concentrations derived from the AMS results were blank corrected following Binnie *et al*. (2019), with resulting ^{10}Be concentrations ranging between 1.69×10^4 and 6.04×10^4 at g^{-1} and ^{26}Al concentrations between 0.821×10^4 and 15.7×10^4 at g^{-1}. Some of the samples, especially those for which limited amounts of quartz were available, required blank corrections amounting to a significant fraction of the total concentration measured. In addition, ^{26}Al counts detected by the AMS were low, particularly for five of the samples. Consequently, five of the 10 measurements were discounted and not used in the age derivation. The remaining five samples have respective ^{10}Be and ^{26}Al blank corrections of less than 16 and 5%. The ratios of the five accepted ^{26}Al/^{10}Be measurements range between 3.54 and 2.59, with an error weighted mean and one standard error of 2.94 ± 0.25. Assuming decay constants of $9.83\pm0.25\times10^{-7}$ year^{-1} (Nishiizumi 2004) and $4.987\pm0.043\times10^{-7}$ year^{-1} (Chmeleff *et al*., 2009; Korschinek *et al*., 2009) for ^{26}Al and ^{10}Be, respectively, and an initial burial ratio of ^{26}Al to ^{10}Be of 6.75, we apply the error weighted mean ratio and the formula for burial times given in Granger & Muzikar (2001) to derive an age and one standard error uncertainty of 1.72 ± 0.15 Ma. Alternatively, if we assume the sediments had a complex exposure history prior to their burial at the core site, i.e. that the ^{26}Al/^{10}Be ratio at the time of burial was less than 6.75, then the sample with the lowest ratio of the five (5045-1D-202A-CC-10) gives the most meaningful age as 1.97 ± 0.48 Ma (1 SD). However, although we use a subset of the more robust measurements, we note that the individual results are close to reliable limits and thus a more definitive age requires further analysis.

Data S1. References used in Supporting Information.